Chapter 3
Synthetic Nanosheets from Ion-Exchangeable Layered Solids

Teruyuki Nakato

3.1 Introduction

Exfoliated inorganic nanosheets of ion-exchangeable layered solids were obtained for the first time from the smectite group of clay minerals, which are natural cation-exchangeable layered crystals consisting of negatively charged aluminosilicate layers with interlayer exchangeable cations [1, 2]. These clay minerals spontaneously undergo infinite swelling in water by taking the solvent into their interlayer spaces when the interlayer cations are Na^+ or Li^+, which can be hydrated to a large extent. The infinite swelling leads to exfoliation of individual layers to yield clay nanosheets. Such interlayer swelling is possible for various other ion-exchangeable layered solids if efficient interactions exist between the interlayer cations and solvent molecules. To date, exfoliation by the interlayer swelling has been realized for numerous synthetic ion-exchangeable layered solids.

Because the ion-exchangeable layered solids include both of cation- and anion-exchangeable materials, we now have a rich library of negatively and positively charged inorganic nanosheets [3–5]. Negatively charged nanosheets are usually obtained by exfoliation of layered oxometallates and metal phosphates, while positively charged ones are prepared from layered hydroxides. The nanosheets possess a wide variety of physicochemical properties. Nanosheets of the oxides, metal phosphates, and hydroxides composed of main-group elements are rather electronically inert and optically transparent. Oxometallates and hydroxides of transition metal and rare-earth elements are often photochemically and electronically active, showing various electric, optic, and magnetic functions.

This chapter describes fundamental aspects of the inorganic nanosheets obtained from ion-exchangeable layered solids other than the smectite group of clay minerals

T. Nakato (✉)
Department of Applied Chemistry, Kyushu Institute of Technology,
1-1 Sensui-cho, Tobata-ku, 804-8550 Kitakyushu, Fukuoka, Japan
e-mail: nakato@che.kyutech.ac.jp

T. Nakato et al. (eds.), *Inorganic Nanosheets and Nanosheet-Based Materials*,
Nanostructure Science and Technology, DOI 10.1007/978-4-431-56496-6_3

that are reviewed in the preceding chapter. It includes details of exfoliation such as the role of exfoliating reagents and delamination mechanisms, the state of the exfoliated nanosheets in the solvents, preparation and structures of nanosheet assemblies, and brief comments on the structure and functions of some typical nanosheet species.

3.2 Cation-Exchangeable Layered Solids and Their Exfoliation

3.2.1 Cation-Exchangeable Layered Solids

Most of the cation-exchangeable layered solids that can be exfoliated into the nanosheets are layered oxometallates and metal phosphates. Table 3.1 lists such materials except for the clay minerals. Structures of these layered solids consist of negatively charged metal oxide or phosphonate layers and interlayer exchangeable cations. For many transition metal-based oxometallates such as titanates, niobates, manganates, and ruthenates, the oxide layers are usually constructed of metal-oxygen (MO_6) octahedral connected by corner- and edge-sharing, while layered silicates are built up from corner-sharing SiO_4 tetrahedra. The metal phosphates layers consist of MO_6 octahedra and PO_4 tetrahedra. These layers have negative charges stoichiometrically determined by their composition. In most cases,

Table 3.1 Representative synthetic ion-exchangeable layered solids that can be exfoliated into nanosheets

Exchangeable ion	Category	Representative compounds	References
Cation	Titanate	$H_xTi_{2-x/4}\square_{x/4}O_4$, $H_{0.8}Ti_{1.2}Fe_{0.8}O_4$, $H_2Ti_3O_7$, $H_2Ti_4O_9$	[6–9]
	Niobate	$K_4Nb_6O_{17}$, HNb_3O_8, $HTiNbO_5$, HTi_2NbO_7, $HNbWO_6$,	[10–14]
	Tantalate	$HTaO_3$, $HTaWO_6$	[13, 15]
	Perovskite-type niobate, tantalate	$HCa_2Nb_3O_{10}$, $HLaNb_2O_7$, $H_2SrTa_2O_7$	[16–18]
	Manganate	$K_xMnO_2{\cdot}nH_2O$	[19]
	Cobaltate	$HCoO_2$	[20]
	Ruthenate	$K_{0.2}RuO_{2.1}$, $Na_{0.22}RuO_2$	[21, 22]
	Tungstate	$H_2W_2O_7$, $Cs_{6+x}W_{11}O_{36}$	[23, 24]
	Silicate	Octosilicate ($Na_8H_8Si_{32}O_{72}{\cdot}32H_2O$)	[25]
	Metal phosphate	α-$Zr(HPO_4)_2$, $H_3Sb_3P_2O_{14}$	[26, 27]
Anion	Layered double hydroxide	$[Mg_{1/3}Al_{2/3}(OH)_2](NO_3)_{1/3}]$ $[Co_{1/3}Al_{2/3}(OH)_2](CO_3)_{1/6}$	[28, 29]
	Hydroxide salt	$Cu_2(OH)_3(CH_3COO){\cdot}H_2O$ $La(OH)_2NO_3$	[30, 31]

the layer charge density is too high to allow spontaneous exfoliation through the interlayer solvation. This situation is overcome by the use of exfoliating reagents as described below.

3.2.2 *Exfoliation*

Cation-exchangeable layered solids are usually exfoliated into nanosheets through exchange of the interlayer cations for appropriate cations that are often called exfoliating reagents. The exfoliating reagents are usually organic cations with appropriate bulkiness and high affinity for the solvent. The exfoliating reagents are first intercalated to the layered crystals through ion exchange, and then drag the solvent molecules into the interlayer spaces (Fig. 3.1). Typically, organic cations represented by tetrabutylammonium ions (TBA^+) are used for the exfoliation in water while long-chain organic species are employed for exfoliation in organic solvents. The organoammonium exfoliating reagents are often intercalated to the layered solids with the aid of acid-base reactions when they cannot be directly incorporated [32]. This method involves acid treatment of the starting layered solids, by the treatment of which the interlayer cations are exchanged for H^+ ions, and subsequent reaction with organic amine molecules that react with the H^+ ions by the acid–base mechanism to form interlayer organoammonium ions that induce exfoliation.

The exfoliation through the ion-exchange route facilitates formation of the single nanosheets. This is guaranteed by the presence of interlayer exchangeable cations located in all the interlayer spaces with the same crystallographic microenvironment because of the stoichiometric distribution of the layer charges; a known exception is hexaniobate ($Nb_6O_{17}^{4-}$) nanosheets as described in Sect. 3.4.2 [33]. The incorporated exfoliating reagents attract solvent molecules equally into all of the interlayer spaces to infinitely swell the interlayer spaces. The driving force for the swelling is solvation of the exfoliating reagents by dipole interactions with water and other polar solvent molecules. As a result of infinite swelling, individual layers of the mother crystals are exfoliated into the nanosheets. Because the obtained nanosheets bear negative charges, exfoliating reagents such as TBA^+ ions are attached to the nanosheets to compensate the layer charge.

In contrast to exfoliation in aqueous systems, that in nonpolar organic solvents has rarely been examined. Such exfoliation can be realized by the use of

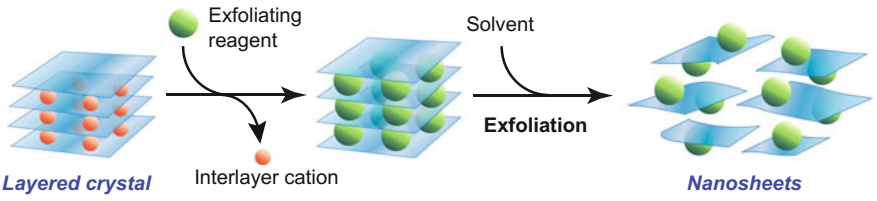

Fig. 3.1 Schematic model of the exfoliation of cation-exchangeable layered solids

organophilic exfoliating reagents such as long-chain organic molecules through hydrophobic interactions with the nonpolar solvents. However, this process is more difficult than exfoliation in water because the inorganic layers themselves are highly polar, and tend to expel the nonpolar solvents because of their electric charges. Although this problem can be overcome by covalent bonding of organic molecules, this technique has only been applied to selected materials as described later.

3.3 Exfoliation Mechanism in Aqueous Systems

According to the systematic studies conducted by Sasaki and coworkers on lepidocrocite-type layered titanate [6, 34–39], $H_xTi_{2-x/4}\square_{x/4}O_4$ ($x \sim 0.7$, $\square$: vacancy) [40–42], osmotic swelling plays a key role in the exfoliation mechanism of cation-exchangeable layered solids in water (Fig. 3.2). This section describes the exfoliation mechanism and important factors affecting the nanosheet generation of the titanate in water as an example of the exfoliation of cation-exchangeable layered solids.

3.3.1 Osmotic Swelling

The exfoliation of cation-exchangeable layered solids begins by gigantic or infinite swelling of the interlayer spaces. Such swelling is generally called osmotic swelling. This concept was proposed in the 1930s and discussed until the 1970s to

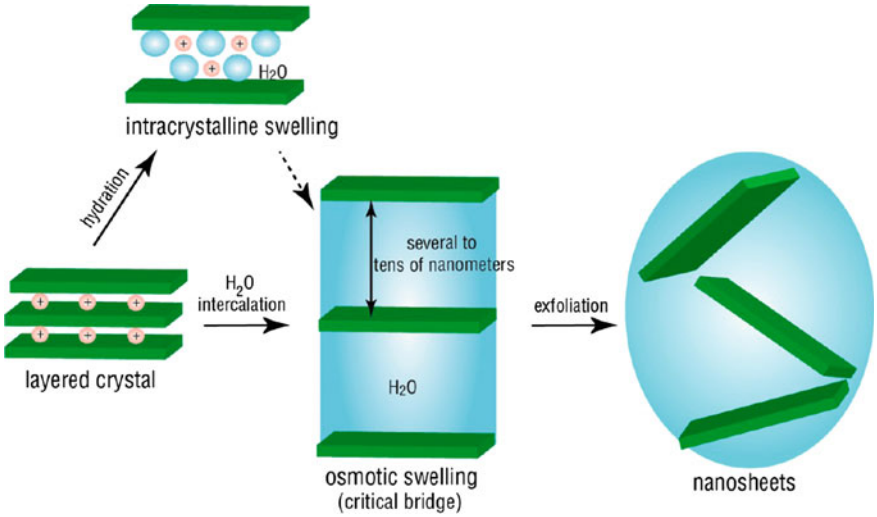

Fig. 3.2 Schematic illustration of the swelling and exfoliation process of lepidocrocite-type titanate. Reprinted with permission from [38]. Copyright 2014 American Chemical Society

explain very high degree of swelling observed for the smectite group of clay minerals in water [1, 2, 43]. For the case of the layered titanate $H_xTi_{2-x/4}\square_{x/4}O_4$, each crystallite effectively draws a huge amount of water molecules into its interlayer spaces through dipole interactions with the interlayer cations when they are TBA^+ ions [6, 35]. As a result, the basal spacing of the titanate layers reaches more than several tens of nanometers, which is more than ten times that of the starting titanate crystal ($\sim$1 nm). However, the amount of incorporated water molecules in the swollen state is too large to be explained by molecular interactions between the interlayer TBA^+ ions and water. In fact, the process is rationalized by the osmotic pressure between the interlayer spaces and outside solvents. Because the hydrated interlayer space is recognized as a TBA^+ solution with a high concentration, a large amount of water molecules outside the interlayer spaces can penetrate into the interlayer spaces driven by the difference in osmotic pressure between inside and outside the interlayer spaces.

In addition to such a qualitative explanation, recent studies on layered titanate $H_{0.8}Ti_{1.2}Fe_{0.8}O_4$ have enabled quantitative understanding of its osmotic swelling. In these studies, swelling by several primary, tertiary, and quaternary organoammonium ions are compared [36–38]. Most of the organoammonium ions show the same amount of incorporation, and the same degree of interlayer expansion induced by the gigantic swelling (Fig. 3.3). In the fully swollen stage, the concentration of organoammonium ions in the interlayer regions, i.e., in the swollen phase gives an osmotic pressure equal to the atmospheric pressure; the outside solvents contain few organoammonium ions under such conditions. These facts indicate that the

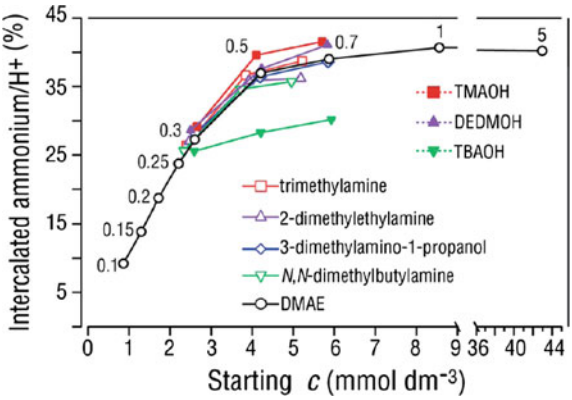

Fig. 3.3 Quantity of intercalated ammonium for tertiary amines and quaternary ammonium hydroxides as a percentage ratio of the cation-exchange capacity (CEC) of the lepidocrocite-type titanate crystals. The *open symbols* represent tertiary amines, while the *filled symbols* represent quaternary ammonium hydroxides. The *numbers* in the panel are the ratios of the starting amine or ammonium hydroxide to the CEC of the crystals. *All lines* except the one for TBAOH overlap, suggesting that these tertiary amines and quaternary ammonium hydroxides have similar affinities for the crystals. The lower intercalation of TBAOH is likely due to steric effects. Reprinted with permission from [38]. Copyright 2014 American Chemical Society

swelling of the layered titanate proceeds until the interlayer osmotic pressure is balanced by the atmospheric pressure. This is the evidence for the osmotic, i.e., colligative nature of the gigantic swelling caused by the organoammonium ions.

3.3.2 From Swelling to Exfoliation

Exfoliation of the cation-exchangeable layered solids is understood as shear-induced liberation of the stacked nanosheets in the gigantically swollen state. The attractive electrostatic interactions between the negatively charged layers through the interlayer cations are weakened under the swollen conditions, and overcome with mechanical shear applied by stirring the solvents. The shear stress causes the exfoliation to form the nanosheets dispersed in the solvent.

Formation of the monolayer (single) nanosheets has been clarified in the exfoliation of lepidocrocite-type titanate $H_xTi_{2-x/4}\square_{x/4}O_4$ [6, 34, 35]. X-ray diffraction (XRD) showed that the basal spacing of the titanate increased while maintaining high stacking regularity upon the intercalation of TBA^+ ions and their hydration as indicated by the shift of the basal reflection accompanied by higher order peaks to lower diffraction angles with maintaining their sharpness. However, when the sample reached the osmotic swelling, the basal reflection disappeared and broad peaks appeared at higher angles. The broad peaks were assigned to the exfoliated monolayer nanosheets according to the X-ray scattering because they were fitted by the square of the structural factor estimated by assuming the single nanosheets. Similar patterns have been obtained following exfoliation of other ion-exchangeable layered solids such as a perovskite-type niobate [44], manganate [45], and layered double hydroxide (LDH) [29]. Their scattering profiles depended on the exfoliated compounds and were fitted by the square of the structural factors of the corresponding nanosheet species (Fig. 3.4).

3.3.3 Effects of the Exfoliating Reagent and Temperature

Regarding the relationship between the interlayer swelling and exfoliation, the osmotic swelling is essentially independent of the exfoliation although the former is a prerequisite for the latter. This relationship has been clarified by studying the swelling of lepidocrocite-type titanate $H_{0.8}Ti_{1.2}Fe_{0.8}O_4$ with different primary, tertiary, and quaternary organoammonium ions [36, 38]. The organoammonium ions that can exfoliate the titanate are limited to several species such as TBA^+, ethylammonium, and propylammonium (PA^+). In contrast, although 2-(dimethylamino) ethanol ($DMAE^+$) gigantically swelled this titanate, it hardly induced the exfoliation even when the swollen titanate powders were mechanically shaken in water (Fig. 3.5). In addition, quaternary TBA^+ and tetramethylammonium (TMA^+) ions

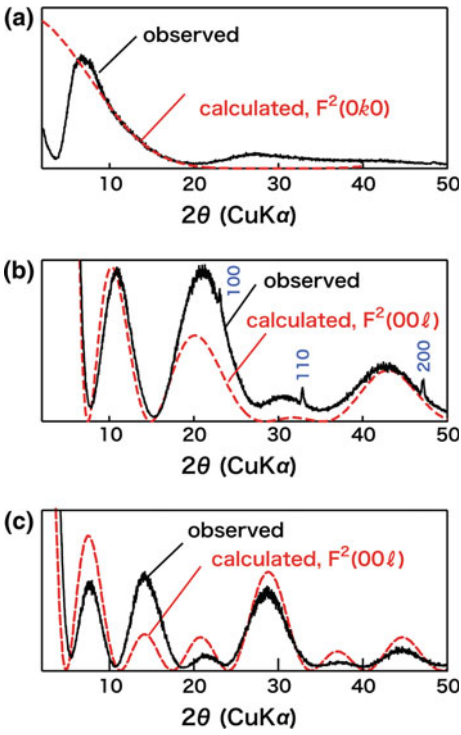

Fig. 3.4 Typical experimental profile of the diffraction envelope (*solid line*) and square of calculated structure factor (*broken line*) for nanosheets. **a** Repidocrocite-type titanate $Ti_{0.91}O_2^{0.36-}$; **b** Perovskite-type niobate $Ca_2Nb_3O_{10}^-$; and **c** Tungstate $Cs_4W_{11}O_{36}^{2-}$. The square of calculated structure factor fits well with the experimental profile. Reprinted with permission from [4]. Copyright 2010 John Wiley and Sons

both exfoliated this titanate, but the former species induced swelling to give unilamellar nanosheets faster than the latter.

These observations indicate that appropriately bulky and moderately polar organoammonium ions work as efficient exfoliating reagents. Cations that are small such as methylammonium and alkali metal cations strongly attaches to the anionic inorganic layers in close proximity in the interlayer spaces, which prohibits hydration of the cations. Highly polar cations such as $DMAE^+$, with positive charges that are localized at the end or edge of the molecules, are thought to strongly interact with water to form hydrogen-bonding networks between the layers to withstand the shear force inducing the exfoliation. A recent study has indicated that organic cations other than the organoammonium species act as the exfoliating reagents of lepidocrocite-type titanate $H_{0.8}Ti_{1.2}Fe_{0.8}O_4$ if the organic species fulfils the above requirement. In fact, tetrabutylphosphonium ions can exfoliate the titanate; they work better than TBA^+ ions because of their bulkiness [39].

Temperature can be another critical parameter affecting the exfoliation. Titanate nanosheets directly synthesized by hydrolysis–polycondensation of a titanium alkoxide in the presence of tetraalkylammonium ions [46] showed reversible exfoliation–stacking behavior under thermal stimuli [47]. The titanate nanosheets prepared by this method were similar to those obtained by exfoliation of tetratitanate $H_2Ti_4O_9$, and dispersed stably in water at room temperature to give a

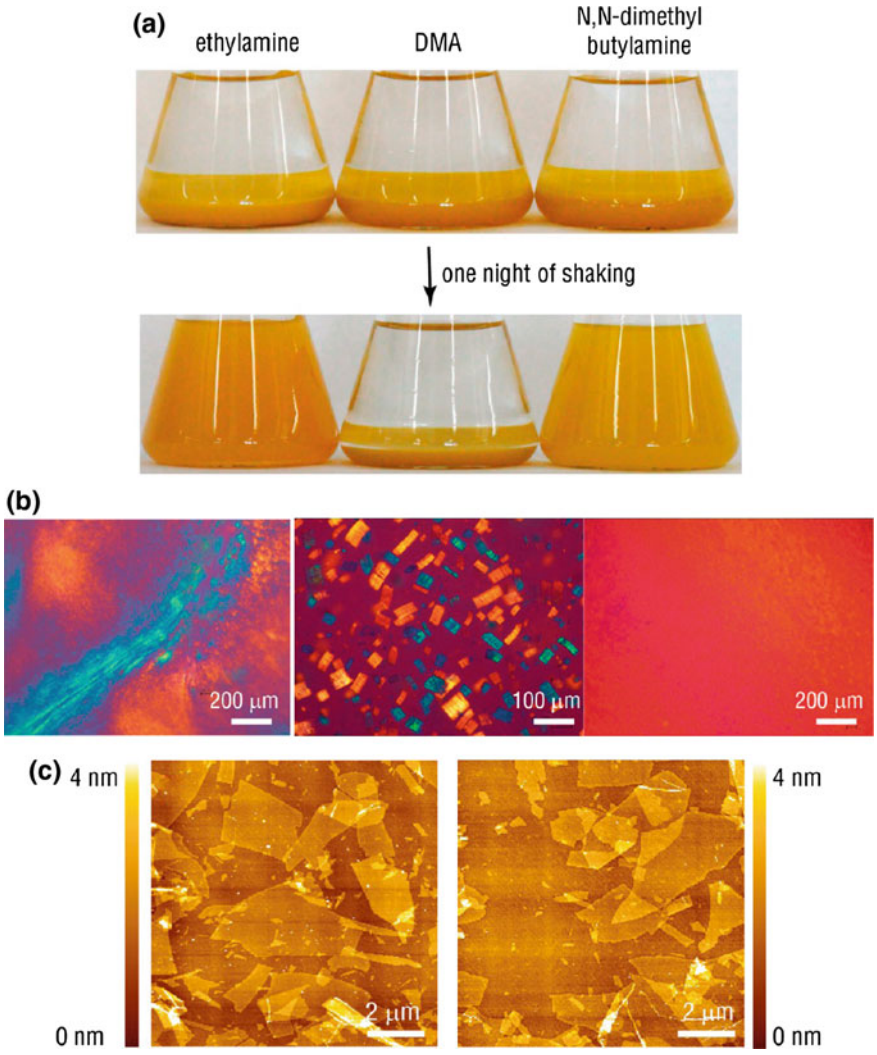

Fig. 3.5 **a** Optical photographs of the crystals swollen with ethylamine, DMA, and *N*,*N*-dimethylbutylamine before and after overnight mechanical shaking. **b** Optical microscopy images of solutions after overnight shaking. *Left* ethylamine, *middle* DMA, and *right* *N*,*N*-dimethylbutylamine. **c** AFM images of delaminated nanosheets in ethylamine and *N*,*N*-dimethylbutylamine. Reprinted with permission from [38]. Copyright 2014 American Chemical Society

transparent colloid. However, these nanosheets were stacked at high temperatures to make the colloid turbid, and were then re-exfoliated by lowering the temperature again. This temperature-induced stacking–exfoliation was reversible for many times, and the transition temperature depended on the tetraalkylammonium species coexisting in the system (Fig. 3.6). This behavior has been ascribed to the

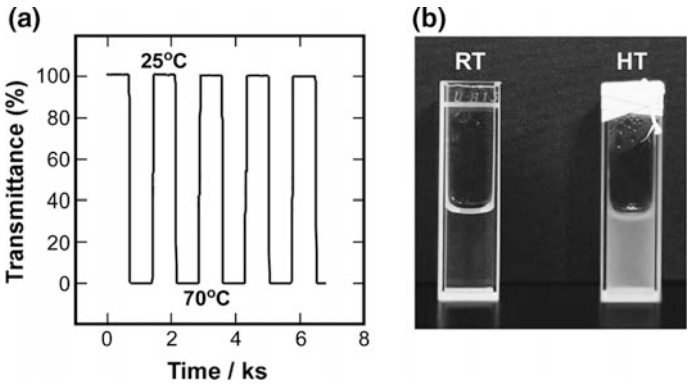

Fig. 3.6 **a** Transient transmittance at 550 nm of TBA^+–TiO_x during temperature switching between 25 and 70 °C. **b** Photographs of TBA^+–TiO_x colloidal solution at room (*RT*) and high temperature (*HT* around 60 °C). Reprinted with permission from [47]. Copyright 2014 Royal Society of Chemistry

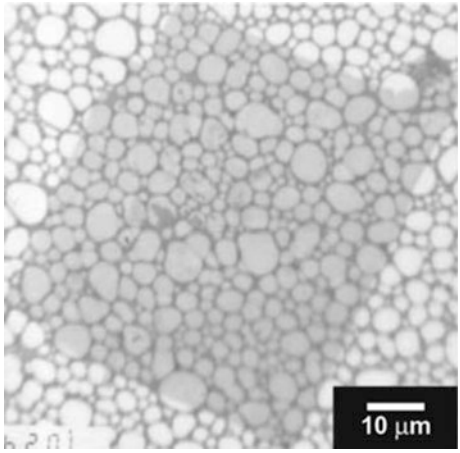

Fig. 3.7 TEM image of a large niobate nanosheet prepared by exfoliation of single crystalline $K_4Nb_6O_{17}$. Reprinted with permission from [33]. Copyright 2002 Royal Society of Chemistry

temperature dependence of the thickness of the electrical double layers at the titanate nanosheets.

3.3.4 Nanosheet Size

The lateral size of the exfoliated nanosheets reflects the size of the mother crystals of the layered solids. Nanosheets with a lateral dimension of micrometers have been obtained from the exfoliation of single crystalline layered titanate $H_xTi_{2-x/4}\square_{x/4}O_4$ [48] and niobate $K_4Nb_6O_{17}$ [33] with a millimeter to centimeter-scale of crystallite size (Fig. 3.7). The size decrease in the lateral direction compared with that of the

starting crystallites is caused by breakage of the nanosheets by the mechanical shear applied during the swelling and exfoliation processes. Since this is unavoidable and uncontrollable in the current experimental techniques for exfoliation, the nanosheets produced have large size distributions in the lateral direction although their thickness is monodisperse because the swelling of the ion-exchangeable layered solids occurs equally in all of the interlayer spaces as described above. The size distribution of nanosheets can be narrowed by gradient centrifugation [49]. The average lateral size of the nanosheets can be reduced by ultrasonic irradiation of the colloidal nanosheets after the exfoliation [50].

3.4 Exfoliation of Typical Cation-Exchangeable Layered Solids

This section briefly describes the structure, exfoliating behavior, and use of the exfoliated nanosheets obtained from typical cation-exchangeable layered solids.

3.4.1 Titanates

Layered titanates are the materials whose exfoliation has been studied the most of various ion-exchangeable layered solids [51], as described Sect. 3.3. These materials consist of negatively charged titanium oxide layers constructed of corner- and edge-shared TiO_6 octahedra and interlayer exchangeable cations [52, 53]. While lepidocrocite-type titanate $H_xTi_{2-x/4}\square_{x/4}O_4$ characterized by the edge-shared connection of TiO_6 octahedra in a flat manner is the most well-known compound [41], other titanates such as trititanate $H_2Ti_3O_7$ and tetratitanate $H_2Ti_4O_9$, both of which have zigzag-shape titanate layers with the corner- and edge-shared TiO_6 octahedra, are also available (Fig. 3.8) [54–58]. For the lepidocrocite-type titanate, Ti atoms in

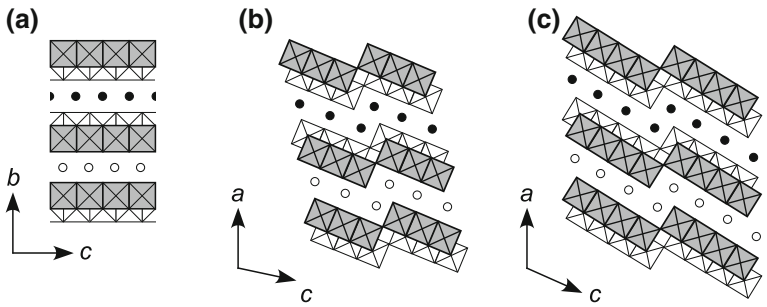

Fig. 3.8 Schematic representation of the crystal structures of **a** lepidocrocite-type titanate $H_xTi_{2-x/4}\square_{x/4}O_4$, **b** $H_2Ti_3O_7$, and **c** tetratitanate $H_2Ti_4O_9$

the layers can be partly substituted with other metallic species such as Mg, Mn, Fe, and Co, as exemplified by $H_{0.8}Ti_{1.2}Fe_{0.8}O_4$ [7, 36, 59–63].

Layered titanates are usually obtained with alkali cations as the interlayer exchangeable cations; e.g., $Cs_xTi_{2-x/4}\square_{x/4}O_4$, $Na_2Ti_3O_7$, and $K_2Ti_4O_9$ [40, 64, 65]. The alkali cations are readily exchanged for H^+ ions by acid treatments, and then the obtained titanic acids react with organoammonium ions as the exfoliating reagent by the acid-base mechanism. While TBA^+ is employed in most cases [6, 9, 34, 35, 66, 67], short-chain organoammonium monocations have been used for trititanate $H_2Ti_3O_7$ and tetratitanate $H_2Ti_4O_9$ [8, 68].

The exfoliation of the layered titanates in organic solvents has been investigated. Tetratitanate $H_2Ti_4O_9$ has been exfoliated in nonpolar solvents such as benzene, chloroform, octanol, and ethylacetate after grafting long-chain organosilyl moieties onto the titanate layers [69, 70]. A recent study has reported that lepidocrocite-type titanate $H_xTi_{2-x/4}\square_{x/4}O_4$ can be exfoliated in toluene after intercalation of tetradecylammonium and octadecylammonium ions (Fig. 3.9) [71].

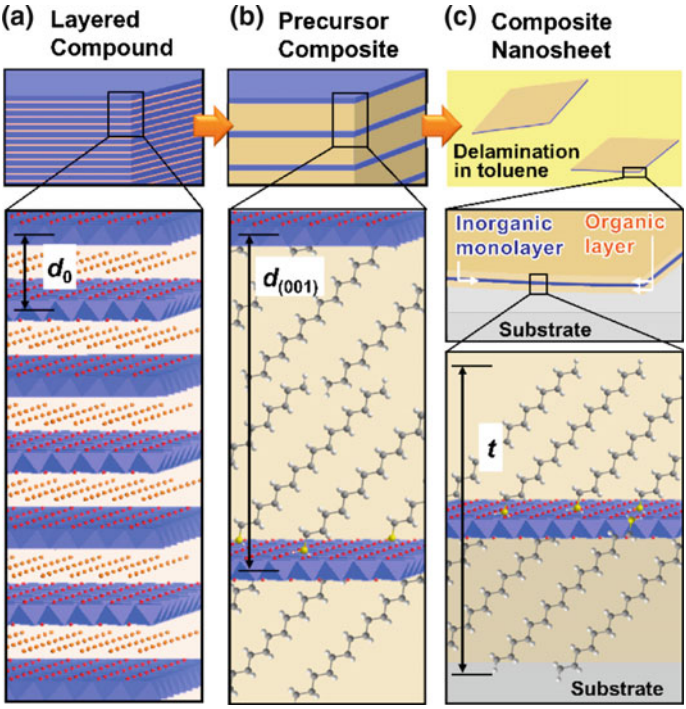

Fig. 3.9 Schematic illustration of the approach for preparing the lepidocrocite-type titanate nanosheets in an organic solvent. **a** The pristine titanate with the interlayer space of d_0; **b** The precursor composite with the intercalation of the long-chain alkylammonium ions in the interlayer space; and **c** The delamination into toluene through the hydrophobic interaction and the formation of the composite nanosheets on a silicon substrate. The $d_{(001)}$ and t indicate the interlayer distance of the precursor composite and the thickness of the composite nanosheets, respectively. Reprinted with permission from [71]. Copyright 2009 American Chemical Society

Applications of the titanate nanosheets by utilizing their wide band-gap semiconducting [72–76] and dielectric properties [4, 77, 78] have been examined. Titanate nanosheets have been investigated as photocatalysts for a long time as described in Chaps. 15–17 [79–84]. Nitrogen- and iodine-doping of lepidocrocite-type titanate nanosheets can narrow their band-gap to result in visible-light photocatalytic activity [85, 86]. In other researches, the titanate nanosheets are employed as dielectric building blocks in electronic devices prepared by layer-by-layer (LbL) assembly of various nanosheets [77, 87]. Lepidocrocite-type titanate nanosheets partially substituted by Mn, Fe, and Co exhibit redox, magnetooptic, and ferromagnetic properties that reflect the nature of dopants [59–62, 88].

3.4.2 Niobates and Tantalates

Layered niobates and tantalates, exemplified by HNb_3O_8, $K_4Nb_6O_{17}$, and $HTaO_3$, possess structures and properties similar to those of the layered titanates [15, 32, 89–93]. Figure 3.10 shows schematic structures of some layered niobates. These materials are constructed from connected NbO_6 or TaO_6 octahedra that form electrically negative layers with interlayer cations. Binary oxometallates including a transition metal in addition to Nb or Ta are also known: e.g., $HTiNbO_5$, $HNbWO_6$, and $HTaWO_6$ [94–98]. Lepidocrocite-type titanoniobate $H_{0.7}Ti_{1.825-x}Nb_xO_4$ (x = 0–0.33) has also been prepared [99]. Most of these layered materials can be exfoliated by the reaction of H^+-exchanged layered crystals with TBA^+ ions [11, 14, 15, 100, 101]. Other reported exfoliating reagents in water are triethanolammonium cations and $NH_2(CH_2)_{10}COOH$ molecules [102, 103]. Fluoroniobate K_2NbO_3F [104] has been reported to be exfoliated in water by an ultrasonic treatment without exfoliating reagents. However, this could be different from ordinary exfoliation because the exfoliated crystals are recovered as $KNbO_3$ with a 3D cubic structure [105, 106].

Among the layered niobates and titanates, hexaniobate $K_4Nb_6O_{17}$ shows special exfoliating behavior. This material is characterized by two types of alternating interlayer spaces called interlayers I and II. The interlayer K^+ ions can be directly exchanged for various cations without acid treatment and those in interlayer I show

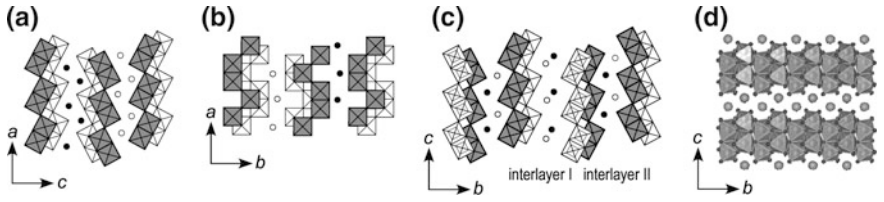

Fig. 3.10 Schematic representation of the crystal structures of **a** $HTiNbO_5$, **b** HNb_3O_8, **c** $K_4Nb_6O_{17}$, and **d** $LiMWO_6$ (M=Nb, Ta). **d** Reprinted with permission from [107]. Copyright 2009 American Chemical Society

higher reactivity than those in interlayer II [91, 108, 109]. Exfoliation induced by treating $K_4Nb_6O_{17}$ with PA^+ ions yielded bilayer nanosheets through swelling of interlayer I, because PA^+ ions displace the K^+ ions only in interlayer I [33, 110, 111]. Exfoliation was also achieved by the two-stage process of acid treatment and subsequent TBA^+ or butylammonium exchange, which also generates the bilayer nanosheets [10, 100, 112, 113].

Exfoliation of the layered niobates in organic solvents has been achieved for $K_4Nb_6O_{17}$ by making the interlayer spaces hydrophobic by grafting long-chain organic moieties onto the niobate layers. Grafting is attained after expanding the interlayer spaces with dodecylammonium ions (DA^+). Because the exchange of K^+ for DA^+ occurred in both interlayers I and II [109], grafting took place in both interlayer spaces to give monolayer nanosheets. Grafting of octadecyltrimethylsilyl groups enabled exfoliation in tetrachloromethane [114]. To graft phenylphosphonate moieties in $K_4Nb_6O_{17}$, interlayer expansion was carried out with dioctadecyldimethylammounium ions in addition to DA^+; the former only expanded interlayer I, while the latter expanded both interlayer spaces. This enabled two types of grafting of phenylphosphonate groups, and provided both of the bilayer and monolayer nanosheets upon exfoliation in acetonitrile (Fig. 3.11) [115].

Niobate and tantalate nanosheets have been used as semiconducting photocatalysts and dielectric materials similar to the titanate nanosheets [10, 78, 87, 102, 116–125]. Photoelectrochemical cells have also been constructed containing these nanosheets [126–128]. In addition, because the acid strength of H^+ ions on the niobate and tantalate nanosheets is greater than those on the titanate nanosheets [32], they have been applied as strong solid acid catalysts [13, 107, 129, 130].

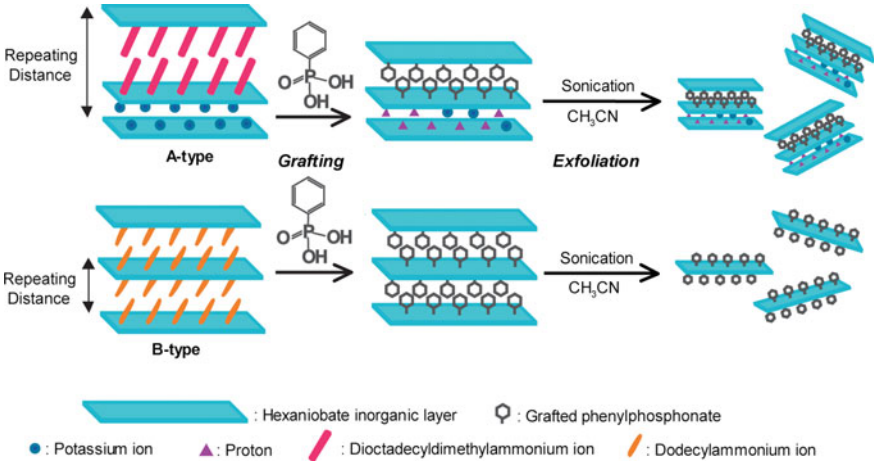

Fig. 3.11 Preparation of monolayer- and bilayer-nanosheets by exfoliation of layered hexaniobate $K_4Nb_6O_{17}$ modified with phenylphosphonic acid. Reprinted with permission from [115]. Copyright 2014 American Chemical Society

3.4.3 Perovskite-Type Titanates, Niobates, and Tantalates

Perovskite-type titanates, niobates, and tantalates are members of cation-exchangeable layered oxometallates characterized by perovskite-type oxide layers [131, 132]. Each perovskite-type layer is a slice of a cubic crystal of ABO_3 perovskite cut in parallel to its (100) direction with containing n B-site sheets (sheets of connected BO_6 octahedra), which sandwiches to interlayer cations such as alkali metal ions to build up the layered structure (Fig. 3.12). The Dion–Jacobson (DJ) phase $M[A_{n-1}B_nO_{3n+1}]$ [133, 134] and Ruddlesden–Popper (RP) phase $M_2[A_{n-1}B_nO_{3n+1}]$ (M=Na, K, etc.; A=Ca, Sr, lanthanide, etc.; B=Ti, Nb, Ta) [135–137] are known. The number of B-site sheets, n, reflects the thickness of a perovskite-type layer; the layer thickness with $n \geq 3$ is much larger than that of the conventional layered titanates, niobates, and tantalates described in the above sections. The interlayer cations are usually exchanged for H^+ ions by acid treatment prior to the exfoliation because the interlayer alkali ions M^+ are strongly held by the perovskite-type layers [138]. Considering the DJ and RP phases, the former incorporates organoammonium ions more easily than the latter because the latter has a higher layer charge density and interlayer cations in more confined environments [139].

Exfoliation of perovskite-type niobate $HCa_2Nb_3O_{10}$ (DJ phase, $n = 3$) has been investigated ahead of other layered titanates, niobates, and tantalates using a commercial monoamine surfactant as the exfoliating reagent [16]. To date, exfoliation of $HCa_2Nb_3O_{10}$ has been frequently carried out mainly with TBA^+ ions [140–143]. Formation of the monolayer nanosheets has been established by the XRD study [44]. Niobates and tantalates with thicker layers, $HCa_2Na_{n-3}Nb_nO_{3n+1}$ (DJ phase, $n = 4$–6), those partially substituted by lantanide elements such as $HLn_{1-x}La_xNb_2O_7$ (Ln = Sm^{3+}, Eu^{3+}, Gd^{3+}, etc.; DJ phase; $n = 2$), and those doped with fluorine and nitrogen such as $HRbSrNb_2O_6F$ (DJ phase, $n = 2$) can also be

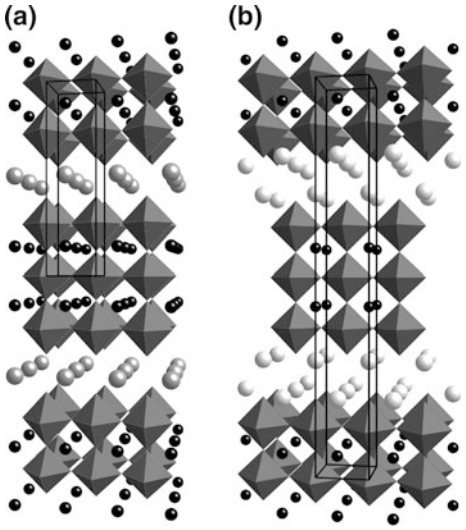

Fig. 3.12 Schematic representations of the crystal structures of perovskite-type layered **a** niobate $RbCa_2Nb_3O_{10}$ (DJ phase, $n = 3$) and **b** titanate $K_2La_2Ti_3O_{10}$ (RP phase, $n = 3$)

exfoliated [144–151]. For the RP phase, $H_2[A_{n-1}B_nO_{3n+1}]$ (A = Na, Ca, Sr, La; B = La, Ti; n = 2 or 3), $H_2SrTa_2O_7$ (n = 2), $H_{1.67}Bi_{0.21}Sr_{0.85}Ta_2O_7$ (n = 2), and $H_2Sr_{1.5}Ta_3O_{10}$ (n = 3) form nanosheets with the aid of organoammonium cations [18, 152–154]. $Li_2Bi_4Ti_3O_{12}$ (RP phase, n = 3) has been exfoliated in water without an exfoliating reagent to yield $[Bi_4Ti_3O_{12}]^-$ nanosheets accompanied by reduction of water [155]. Exfoliation in organic solvents has been achieved for $HLaNb_2O_7$ by grafting a siloxane-terminated polymers and alkoxysilane through controlled hydrolysis–condensation reactions [17].

Applications of the perovskite-type oxometallates are similar to those of the other layered titanates, niobates, and tantalates described above. Photocatalysts, photoelectrodes, and photoconductive films of the perovskite-type nanosheets have been prepared [44, 128, 156–166]. The dielectric properties of such nanosheets have also been utilized [167–169]. Rare-earth substituted nanosheets have been examined as photoluminescent materials [144–147, 150, 153].

3.4.4 Other Transition-Element Oxometallates

3.4.4.1 Manganates

Layered manganate with the birnessite-type structure $A_xMnO_2{\cdot}nH_2O$ (A=Na, K), also known as δ-MnO_2, has been exfoliated to yield manganese oxide nanosheets. The layered structure consists of anionic manganese oxide layers of edge-shared MnO_6 octahedra and interlayer cations (Fig. 3.13) [170–172]. Sodium manganate synthesized by oxidation of Mn^{2+} species in an alkaline solution [19, 173] and potassium manganate prepared by oxidation of Mn_2O_3 through calcination [45, 174] or by reduction of permanganate ions with KOH are used as the starting materials of the nanosheets [175]. After exchange of the interlayer alkali ions for H^+ ions, the layered manganate is exfoliated with the aid of TBA^+ or TMA^+ ions. Complete exfoliation to monolayers was established by the XRD analysis. In addition, the manganate nanosheets have been directly synthesized by oxidation of Mn^{2+} ions in the presence of TBA^+ ions [176]. Because of the mixed-valent and

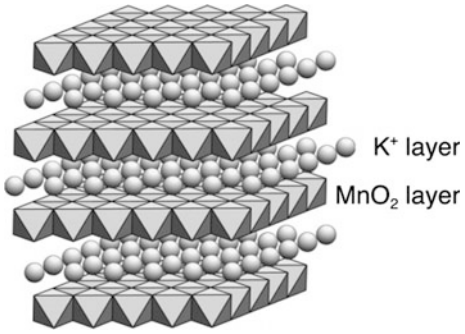

Fig. 3.13 Schematic representation of the crystal structure of layered manganate $K_{0.45}MnO_2$. Reprinted with permission from [174]. Copyright 2006 American Chemical Society

redox-active nature of the manganese oxides, the manganate nanosheets are applicable to electrochemical devices such as supercapacitors and lithium-ion batteries [175, 177, 178].

3.4.4.2 Cobaltates

Since layered lithium cobaltate $LiCoO_2$ is known as an electrode material of lithium-ion batteries [179–181], exfoliation of layered cobaltates has been investigated. $LiCoO_2$ has an α-$NaFeO_2$-type structure, which is related to the rock salt structure and consists of $[CoO_2]^-$ layers and interlayer Li^+ ions [182] (Fig. 3.14). $LiCoO_2$ has been exfoliated by the acid treatment and successive reaction with TMA^+ ions [20]. Multicomponent cobaltate $Li[Mn_{1/3}Co_{1/3}Ni_{1/3}]O_2$ and nonstoichiometric cobaltate Na_xCoO_2 have also been exfoliated in a similar manner [183]. The exfoliated cobaltate nanosheets are promising for use in lithium-ion batteries, although detailed results have not appeared yet. In addition, the p-type wide band-gap semiconducting nature of the cobaltate [184] is attractive because many other semiconducting oxometallates, such as titanates and niobates, are n-type. Nanosheets prepared from Na_xCoO_2 exhibited thermoelectric properties after reconstruction of the layered structure with Ca^{2+} ions [185].

3.4.4.3 Ruthenates

Inspired by the excellent properties of RuO_2 as an electrochemical capacitor [186], exfoliation of layered ruthenates has been investigated. The first ruthenate exfoliated was $K_{0.2}RuO_{2.1}$ whose structure has not been determined [21]. Exfoliation was

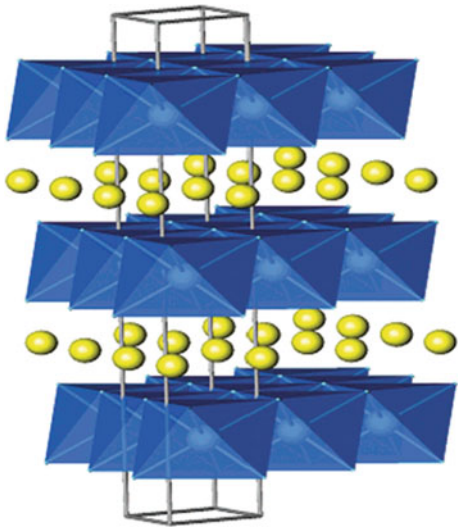

Fig. 3.14 Schematic representation of the crystal structure of layered manganate $LiCoO_2$. Reprinted with permission from [181]. Copyright 2004 American Chemical Society

realized by acid and subsequent TBA^+ treatment. $NaRuO_2$ with an α-$NaFeO_2$-related structure was also exfoliated by the same method after oxidative deintercalation of Na^+ ions to $Na_{0.22}RuO_2$ [22]. The ruthenate nanosheets exhibited superior performance as an electrochemical capacitor compared with that of bulk RuO_2 crystals. A metal–insulator–metal structure applicable to an ultrathin capacitor has been obtained by combining the $Ru_{0.95}O_2^{0.2-}$ and dielectric $Ca_2Nb_3O_{10}^-$ nanosheets [168].

3.4.4.4 Tungstates

Exfoliation of layered tungstates has been reported for $H_2W_2O_7$, which is obtained from $Bi_2W_2O_7$ possessing an Aurivillius-type perovskite structure with vacant A-sites by abstraction of the $Bi_2O_3^+$ unit through an acid treatment [23]. The protonated tungstate was exfoliated through reaction with TBA^+ ions. Exfoliation of layered tungstate $Cs_{6+x}W_{11}O_{36}$ was also achieved by acid and subsequent TBA^+ treatment. In this case, mesh-like tungstate nanosheets with interconnected pyrochlore-type channels were obtained (Fig. 3.15), and the nanosheets show photochromic behavior like that of WO_3 [24].

3.4.5 Silicates

Layered silicates are oxides consisting of anionic silicate layers constructed of corner-shared SiO_4 tetrahedra and interlayer exchangeable cations [187–189]. The structure of layered silicates can be recognized by the numbers of the sheets of

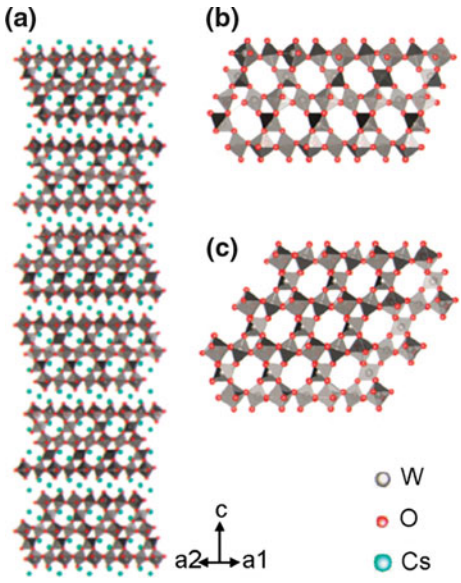

Fig. 3.15 Crystal structure of $Cs_{6+x}W_{11}O_{36}$ viewed along the [110] direction, **a** Pyrochlore-type channels appeared in **b** the section view and in **c** the plane view (a 35° tilt from the horizontal alignment); Cs ions are omitted to highlight the channel structure. Reprinted with permission from [24]. Copyright 2008 American Chemical Society

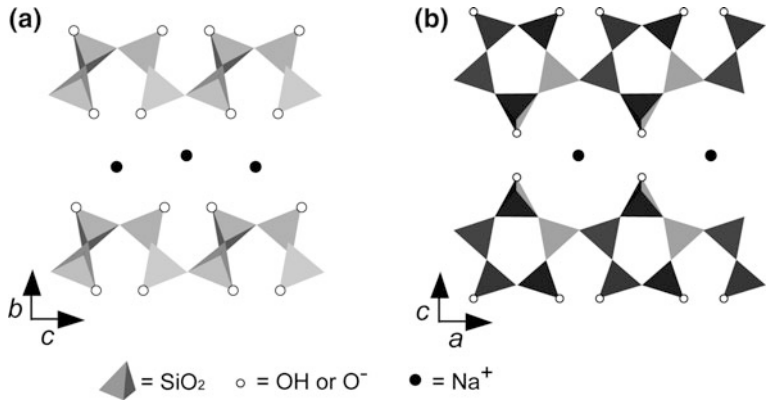

Fig. 3.16 Schematic representation of the crystal structures of **a** kanemite (single-sheet silicate) and **b** octosilicate (double-sheet silicate)

connected SiO_4 tetraheda stacked in each oxide layer. While kanemite $NaHSi_2O_5{\cdot}3H_2O$ and apophyllite $KCa_4[Si_4O_{10}]_2(F, OH){\cdot}38H_2O$ are single-sheet silicates [190, 191], octosilicate $Na_8H_8Si_{32}O_{72}{\cdot}32H_2O$ is a double-sheet silicate [192] (Fig. 3.16). Magadiite has thick silicate layers (more than three sheets), although its crystal structure has not been determined [193]. From a physicochemical point of view, the layered silicates are chemically stable and optically transparent similar to the clay minerals but they do not show specific electronic and photochemical properties. Such properties are different from those of the transition-metal oxometallates described above.

Although the cation-exchangeable layered silicates intercalate many guest molecules through various mechanisms including cation exchange, acid-base reaction, polar adsorption, and grafting, they do not show high exfoliating reactivity. There is no reliable report of the TBA^+-induced exfoliation of a silicate in water. Exfoliation of octosilicate in water has been realized by multistep modification of the silicate layers; the Si–OH groups on the layer surfaces were grafted with organosilyl moieties possessing mercapto terminal groups, and then the terminals were oxidized to hydrophilic $–SO_3H$ groups [25]. Grafting of a silane coupling reagent with imidazolium functional groups has also enabled exfoliation of octosilicate in water (Fig. 3.17) [194]. As for exfoliation in an organic solvent, silylation of apophyllite has been reported to give transparent gels of the silicate nanosheets in CCl_4 [195].

3.4.6 Metal Phosphates

Metal phosphates are water-insoluble acidic salts obtained form multivalent metal ions with amphoteric nature, such as Zr^{4+}, Ti^{4+}, Al^{3+}, and Sb^{5+}, and phosphoric

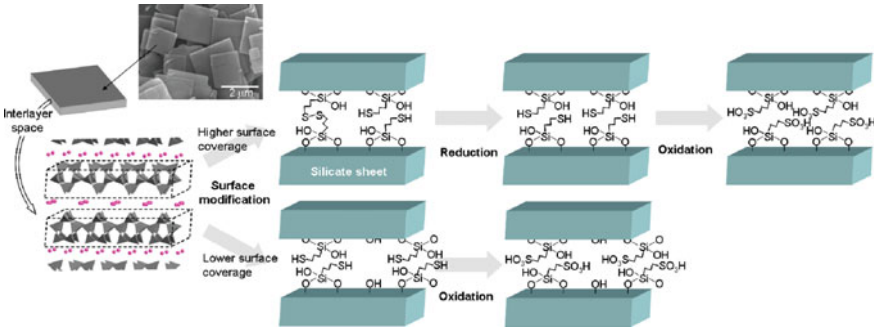

Fig. 3.17 Surface modification of octosilicate with the sulfonic acid group for exfoliation in water. Reprinted with permission from [25]. Copyright 2009 American Chemical Society

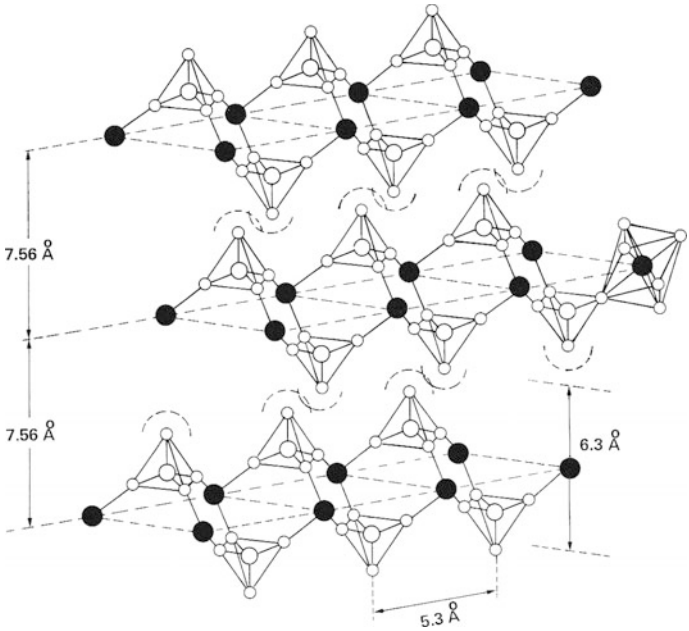

Fig. 3.18 Schematic representation of the crystal structure of α-ZrP. Reprinted from [199]. Copyright 1982 Elsevier Inc

acid. Among various cation-exchangeable amorphous metal phosphates, α-zirconium phosphate (α-$Zr(HPO_4)_2$, α-ZrP) was first found to exist as a layered solid [196]. Various cation-exchangeable layered metal phosphates have since been synthesized. Their structures are characterized by the connection of the MO_6 octahedra and PO_4 tetrahedra to form negatively charged layers (Fig. 3.18). Interlayer exchangeable cations, e.g., H^+ ions for α-ZrP, are held by the $P–O^-$ moieties on the layer surfaces. Layered metal phosphates exhibit high intercalating reactivity through various mechanisms similar to that of layered silicates [197, 198].

In 1985, α-ZrP was found to form a stable colloid in water after reaction with PA^+, which is recognized as the first example of the exfoliation of a layered metal phosphate [26]. Later, formation of α-ZrP nanosheets was confirmed by exfoliation using TBA^+ or a commercial surfactant [100, 200]. γ-ZrP, a polymorph of α-ZrP, can also be exfoliated in water using dimethylamine as the exfoliating reagent [201]. Meanwhile, α-ZrP nanosheets in an aqueous colloidal state after exfoliation with PA^+ underwent sol–gel transition of the colloid upon displacing the solvent (water) for an organic one such as *N*,*N*-dimethylformamide, *N*-methylformamide, tetrahydrofuran, alcohols, or chloroform [202].

Exfoliation of metal phosphates has been extended to materials other than ZrP. Among these materials, layered antimony phosphate $H_3Sb_3P_2O_{14}$ [203] is important because it is exfoliated in water without the aid of an exfoliating reagent. Exfoliation is induced by dialyzing $H_3Sb_3P_2O_{14}$ obtained by acid treatment of $K_3Sb_3P_2O_{14}$ in water [27]. Complete exfoliation to monolayer nanosheets is supported by the liquid crystallinity of the resulting nanosheet colloid (see Chap. 8). Layered aluminophosphate $(C_2H_5NH_3)_3Al_3P_4O_{16}$ was also directly delaminated in a water–ethanol mixture [204]. Ultrasound irradiation assisted exfoliation of iron phenylphosphate $Fe(OH)(C_6H_5PO_4H)_{1.6}(HPO_4)_{0.4}$ in water and olivine-type iron phosphate NH_4FePO_4 in formamide [205]. In contrast, exfoliation of α-titanium phosphate and α-tin phosphate was realized using TBA^+ in acetonitrile [206].

3.4.7 Other Cation-Exchangeable and Related Materials

There are a few layered oxides that can be exfoliated through appropriate interlayer modifications. Although layered oxovanadium phosphate $VOPO_4{\cdot}2H_2O$ is not ion-exchangeable, it can intercalate various polar organic molecules including alcohols and amines [207]. Exfoliation occurs in polar organic solvents after intercalation of aromatic 4-butylaniline or acrylamide [208, 209]. Layered cuprate $Bi_2Sr_2Ca_{m-1}Cu_mO_y$, known as a high-temperature superconducting oxide having a perovskite-related structure, can also be exfoliated [210, 211]. After the starting cuprate was intercalated with HgX_2 (X=Br, I), and then with alkylpyridinium iodide, the material was exfoliated in acetone. Exfoliation of layered molybdate $Na_{0.9}Mo_2O_4$ in water was realized by conventional acid and TBA^+ treatment [212].

Layered solids that do not intrinsically have exchangeable cations can be converted to cation-exchangeable materials through reductive intercalation of interlayer cations. The reduced materials have nonstoichiometric interlayer charges with a low density compared with that of the stoichiometric compounds, and the interlayer spaces can often be infinitely swollen spontaneously like clay minerals. For example, $Fe^{III}OCl$ can be reduced by Fe^0 to $Fe^{II}_{x/2}[Fe^{II}_xFe^{III}_{1-x}]OCl$. The intercalated Fe^{2+} ions are exchangeable, and the interlayer space is swelled infinitely in water [213]. Many transition-metal dichalcogenides can be intercalated with alkali cations such Li^+ and Na^+ through partial reduction of the chalcogenide layers [214].

Solvation of the cations in polar solvents yields colloidal dispersions of the chalcogenide nanosheets [215].

3.5 Exfoliation of Anion-Exchangeable Layered Solids

The library of anion-exchangeable layered solids is still not as rich as that of cation-exchangeable ones. Anion-exchangeable layered solids are classified into LDHs and layered hydroxide salts, and the former is more common than the latter. Exfoliation of these anion-exchangeable layered solids yields positively charged nanosheets, which are important as the counterparts of the negatively charged nanosheets obtained from the cation-exchangeable materials.

3.5.1 Layered Double Hydroxides (LDHs)

LDHs are binary metal hydroxides with a general formula of $[M^{2+}_{1-x}M^{3+}_{x}(OH)_2][X^{m-}]_{x/m}{\cdot}nH_2O$, where M^{2+} and M^{3+} are metal ions and X^{m-} is an interlayer exchangeable anions. Usually, M^{2+} is Ca^{2+}, Mg^{2+}, Fe^{2+}, Ni^{2+}, or Zn^{2+}, M^{3+} is Al^{3+}, Cr^{3+}, Mn^{2+}, Fe^{3+}, or Gd^{3+}, and X^{m-} is $CO_3{}^{2-}$, $SO_4{}^{2-}$, Cl^-, or $NO_3{}^-$. Combination of Li^+ and Al^{3+} is also possible. Organic anions such as carboxylate and sulfonate can also be the X^{m-} species. LDHs are easily synthesized by liquid phase reactions under ambient conditions: typically, controlled precipitation of M^{2+} and M^{3+} species in an alkaline solution. Investigations of LDHs began before the 1940s and their structure and anion exchange behavior were clarified until the 1980s [216–220]. Today, chemical science of LDHs has been grown into a large research field in materials chemistry, and many review articles and books on LDHs have been published [4, 221–225]. Exfoliation of LDHs has also been summarized in detail in a recent review [226], which complements the present section.

The most ubiquitous LDH is $[Mg_{1-x}Al_x(OH)_2](CO_3)_{x/2}$ (Mg–Al–CO_3 LDH), known as hydrotalcite. The layered structure of Mg–Al LDHs is derived from that of brucite $Mg(OH)_2$, which has hexagonal layers consisting of connecting MgO(OH) octahedra. Although the hydroxide layers of brucite are attracted by van der Waals interactions, partial isomorphous substitution of Mg^{2+} for Al^{3+} in Mg–Al LDHs generates positive charges in the layers to allow electrostatic stacking with the interlayer anions for charge compensation. Such electrostatic layering is also observed for other LDHs; nevertheless, they are classified into hexagonal and rhombohedral polymorphs (Fig. 3.19) [216, 222]. The interlayer anions of LDHs are exchanged for many other inorganic and organic anions. However, $CO_3{}^{2-}$ is highly selective compared with other anions, particularly inorganic ones. Thus, selection of the initial interlayer anion is important to accomplish the desired anion exchange.

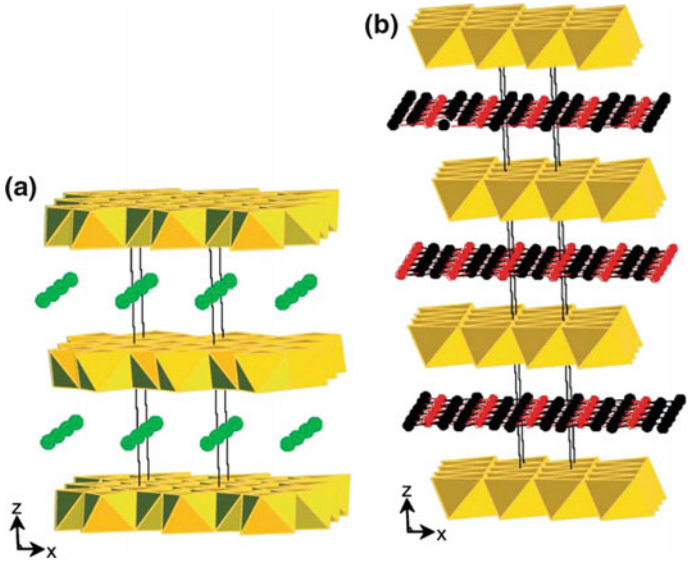

Fig. 3.19 Schematic representation of the crystal structure of an LDH showing the polymorphic stacking patterns: **a** hexagonal, **b** rhomohedral. Reprinted with permission from [222]. Copyright 2002 Royal Society of Chemistry

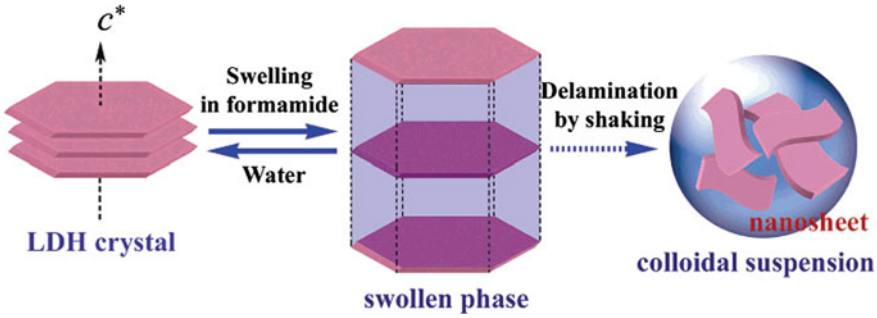

Fig. 3.20 Schematic model of the possible exfoliation mechanism for LDHs in formamide. Reprinted with permission from [29]. Copyright 2006 American Chemical Society

Although exfoliation of LDHs has been achieved by various methods since its discovery in 2000 [227], treating LDHs with interlayer NO_3^- anions in formamide is the most common method today [228]. In the first study of this method, Mg–Al–NO_3^- LDH prepared by a hydrothermal reaction of $Mg(NO_3)_2$ and $Al(NO_3)_2$ in the presence of hexamethyleneteramine was mechanically shaken in formamide [28]. Exfoliation into unilamellar LDH nanosheets through osmotic swelling has been confirmed by the XRD measurements, as mentioned in Sect. 3.3.2. Figure 3.20 schematically illustrates the exfoliation process in formamide. The use

of hexamethylenetetramine as the alkaline reagent and the high reaction temperature under hydrothermal or refluxing conditions yielded large LDH crystallites and thus large exfoliated nanosheets with a lateral dimension of micrometers. The formamide method has been rapidly expanded to a wide range of LDHs such as Co–Al–NO_3^- LDH prepared from other routes like conventional coprecipitation [29, 229, 230]. Other interlayer anions such as CO_3^{2-}, ClO_4^-, and amino acids also tolerate exfoliation in formamide; in fact, amino acids were identified as appropriate anions for formamide prior to NO_3^-.

LDHs incorporating long-chain organic species, e.g., dodecylsulfate anions, as an exfoliating reagent are exfoliated in organic solvents. The interlayer organic anions are introduced by anion exchange from inorganic anions or direct synthesis before exfoliation. Various organic solvents, from polar butanol and acrylate to nonpolar toluene and tetrachloromethane, are available for exfoliation [227, 231–233]. Exfoliation of dodecylsulfate-intercalated LDHs in toluene causes gelation of the solvents (Fig. 3.21) [234, 235]. Borate anions can also be utilized as the exfoliating reagent of LDHs for exfoliation in nonpolar hydrocarbons [236].

Exfoliation of LDHs in water can be achieved by introducing carboxylate anions such as lactate, acetate, and formate into their interlayer spaces [237–240]. Hydrogels were obtained upon exfoliation of Mg–Al–acetate LDH in water. For the case of Mg–Al–methoxide LDH, addition of water causes hydrolysis of the methoxide species in the interlayer spaces, and the hydrolysis induces exfoliation in water [241]. LDHs with interlayer perchlorate anions have been exfoliated in an aqueous solution of amino acids [242].

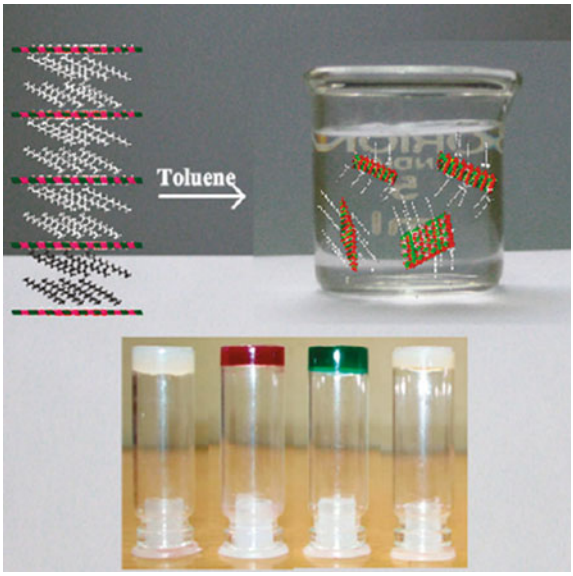

Fig. 3.21 Schematic representation of the exfoliation of organically modified LDHs in toluene and photographs of the gelled nanosheet colloids. Reprinted with permission from [234]. Copyright 2006 American Chemical Society

Like the nanosheets of cation-exchangeable layered solids such as clay minerals and oxometallates, exfoliated LDH nanosheets have been examined for various applications. Specific functions have been designed by the combination of divalent and trivalent metal cations in the LDHs and the positively charged nature of the nanosheets. Although Mg–Al LDHs are chemically inert, those containing transition metals show a variety of physicochemical properties. Redox-active LDHs are obtained with Ni^{2+}, Co^{2+}, and Mn^{2+}, and they have been prepared and examined in supercapacitors and lithium-ion batteries [243, 244]. LDHs with Cr^{3+} and Fe^{3+} have optical absorption in the visible region, and thus exhibit photocatalytic activities [245, 246]. In addition, the positively charged nature of LDH nanosheets allows them to be used as supports of anionic functional molecules that are luminescent, thermochromic, piezochromic, or photosensitizing molecules [247–250]. The positively charged nanosheets can also be used as macro-countercations of the negatively charged oxometallate nanosheets to yield heterocoagulated and superstructured nanosheet assemblies [251, 252]. Used as supports or carriers of bioactive molecules such as proteins, genes, and drugs [253–255] based on the biocompatibility of Mg–Al and Zn–Al LDHs [256, 257] is another growing field.

3.5.2 *Layered Hydroxide Salts*

There are metal hydroxide salts (or metal basic salts) that possess anion-exchangeable layered structures. A typical example is copper hydroxyacetate (basic copper acetate) $Cu_2(OH)_3(CH_3COO)\cdot H_2O$, also known as botallackite [258, 259]. In this compound, acetate groups coordinated to Cu^{2+} in the hydroxide layers are projected into the interlayer spaces, and are partly exchanged for other anions. This layered hydroxide salt can be exfoliated in formamide under solvothermal conditions to yield CuO nanosheets [30]. Analogs of this compound with long-chain carboxylates $M^{II}(OH)_3(C_nH_{2n+1}COO)$ (M^{II} = Cu, Ni, Co; n = 17, 19, 21) are swollen and stably dispersed in toluene, suggesting exfoliation occurs [260]. This system is characterized by colloidal liquid crystallinity. Layered zinc hydroxybenzoate $Zn(OH)_{1.66}(C_6H_5COO)_{0.34}$, which is structurally different from the botallackite analogs, has been exfoliated in C_3–C_5 alcohols [261].

Another class of layered hydroxide salts subjected to exfoliation is lanthanide hydroxides $Ln_2(OH)_3[A^{m-}]_{1/m}$ (Ln = lanthanide; A^{m-} = interlayer anion such as Cl^- and NO^{3-}). Although basic salts of lanthanides have been known for a long time [262, 263], they have recently been rediscovered as anion-exchangeable layered solids [264–266]. Their luminescent and magnetic properties originating from the lanthanide ions have activated this research [264, 266]. Nanosheets of these compounds are also attracting interests in this trend. Exfoliation of layered lanthanide hydroxides has been accomplished by intercalating dodecylsulfate ions through anion exchange and subsequent agitation in formamide (Fig. 3.22) [31, 267].

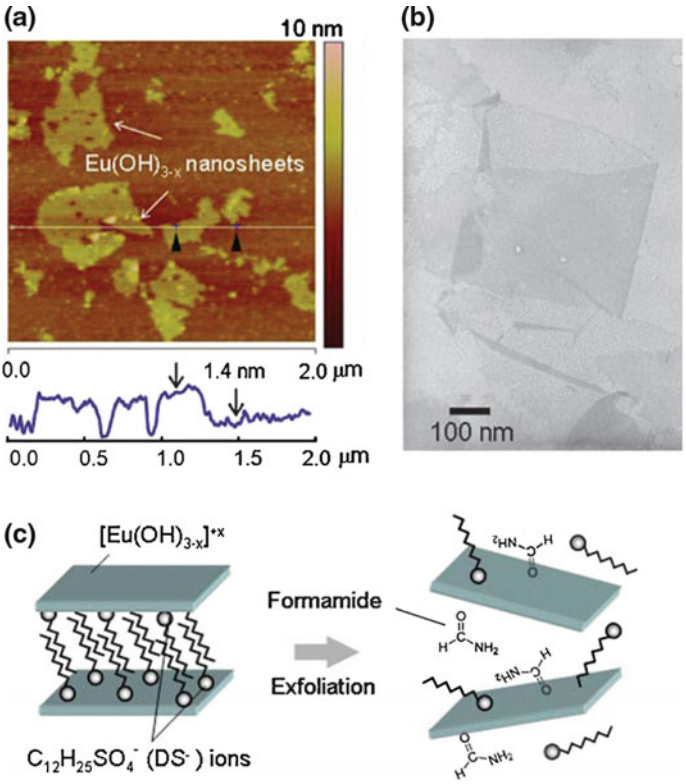

Fig. 3.22 **a** AFM image, **b** TEM image, and **c** model of the preparation process for $Eu(OH)_{3-x}$ nanosheets. Reprinted with permission from [31]. Copyright 2002 Royal Society of Chemistry

3.6 Assembly of the Nanosheets

The exfoliated nanosheets obtained from ion-exchangeable layered solids can be used in practical applications by assembling them appropriately. Employing each nanosheet as a building block, we can construct various nanostructured materials. Nanosheets with different physicochemical properties can be integrated with themselves or other species, including molecules, polymers, and nanoparticles to yield desired materials by fusion of their structures and functions. In such nanosheet assemblies, the electric charges and 2D morphology of the nanosheets play vital roles. Various nanostructures have been organized through electrostatic interactions between the nanosheets, and their 2D shape readily leads to anisotropic nanostructures. The colloidal and interfacial properties of the nanosheets are also important because the nanosheets are usually manipulated in solvents. This section briefly summarizes research on nanosheet assemblies, which are classified into three types based on their preparation techniques.

3.6.1 Aggregation to Bulk Solids

3.6.1.1 Porous Solids

Evaporation of the solvent from colloidal nanosheets usually causes reformation of the layered structure through restacking of the nanosheets. However, porous structures with high surface areas can be obtained if the restacking is appropriately interrupted. To ensure pore generation, templates or pillaring reagents are often used in the aggregation processes. As a direct method without templates, disordered porous aggregates of clay nanosheets with "house-of-cards" structure have been produced [1]. This structure has been obtained by aggregation of small clay nanosheets through face-to-edge electrostatic interactions between them.

For oxometallate and metal phosphate nanosheets, aggregates with high surface areas have been prepared from the nanosheets of, for example, lepidocrocite-type titanate $H_xTi_{2-x/4}\square_{x/4}O_4$, perovskite-type niobate $HCa_2Nb_3O_{10}$, and α-ZrP without the aid of templates [268–270]. Flocculation of titanate nanosheets with Keggin-type $[Al_{13}O_4(OH)_{24}(H_2O)_{12}]^{7+}$ (Al_{13}^{7+}) cations yielded pillared porous structures with a high surface area (>200 $m^2\ g^{-1}$) [271, 272]. Aggregation with metal or oxide nanoparticles is also an effective approach to generate porous structures (Fig. 3.23) [10, 273]. However, hybridization with inorganic nanoparticles has attracted more attention from a functional viewpoint. Based on their cocatalyst or visible-light antenna functions, hybridization with titanate and niobate nanosheets has led to advanced photocatalysts [157, 274, 275].

Deposition of the nanosheets onto polystyrene (PSt) particles yielded core-shell and macroporous aggregates [276]. Removal of the PSt particles by calcination produced macroporous structures. However, the final structure depended the relative size of the nanosheets and PSt particles. While using nanosheets larger than the PSt particles yielded disordered pores with crumpled nanosheets, employing smaller nanosheets than the PSt particles formed ordered pores reflecting the colloidal crystallinity of the PSt particles. A recent study revealed that surfactant micelles can also act as macropore templates in nanosheet aggregates (Fig. 3.24) [277].

Heterocoagulation of negatively charged nanosheets such as titanate with cationic species is also a useful method to aggregate nanosheets into specific structures. Although disordered aggregates are generally obtained upon mixing negatively and positively charged colloidal nanosheets [278], aggregates with layered structures have been obtained for mixtures of lepidocrocite-type titanate or perovskite-type niobate with LDH nanosheets (Fig. 3.25) [251]. The titanate or niobate nanosheets and LDH nanosheets are stacked by sandwiching with each other. The basal spacing determined by XRD analyses corresponded to the sum of the monolayer thicknesses of titanate or niobate and LDH nanosheets, confirming the alternating stacking of nanosheets. Meanwhile, heterocoagulation of lepidocrocite-type titanate nanosheets with biomolecules can improve the functions of the biomolecules. One example is the stabilization of enzyme molecules by the

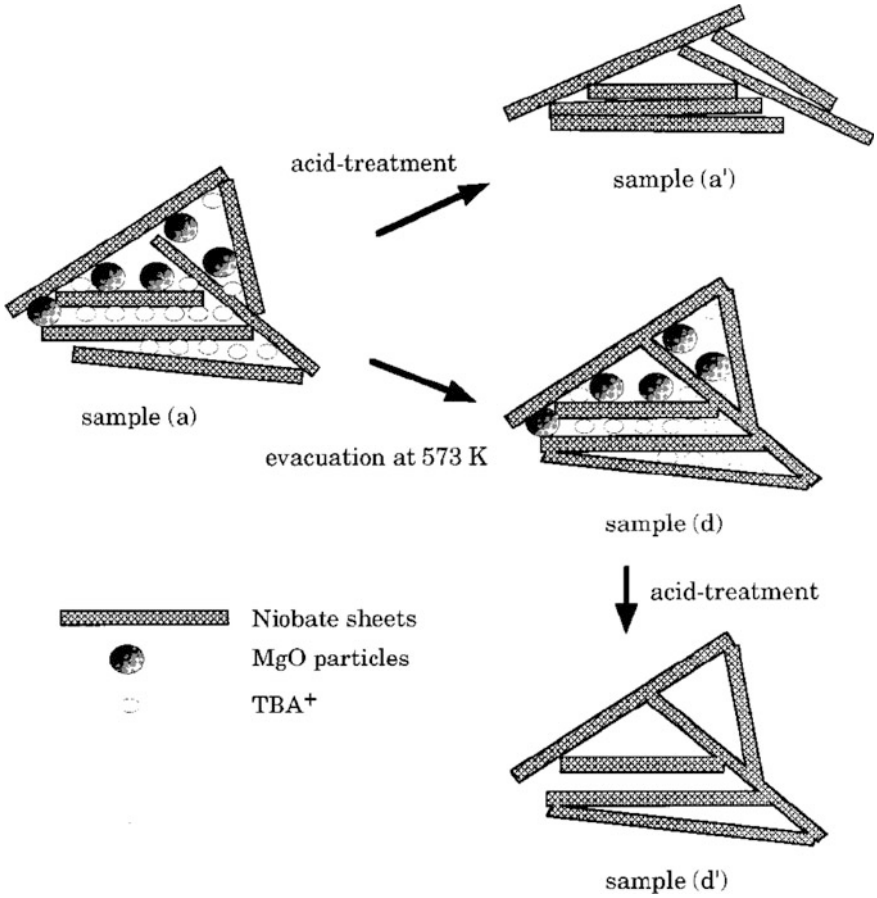

Fig. 3.23 Schematic illustration of the formation of porous structures by aggregation of niobate nanosheets in the presence of oxide nanoparticles. Reprinted with permission from [10]. Copyright 1997 American Chemical Society

titanate nanosheets against UV light exposure [279]. Another example is that antibody molecules immobilized on the nanosheets underwent antigen recognition [280].

3.6.1.2 Cast Films

Deposition of nanosheets onto flat substrates generally produces films because of their 2D morphology. Such nanosheet films are usually prepared by drop- or spin-casting on a substrate [281–284]. Electrophoretic deposition of titanate, cobaltate, and LDH nanosheets has also been reported [9, 20, 285]. Nanosheet films

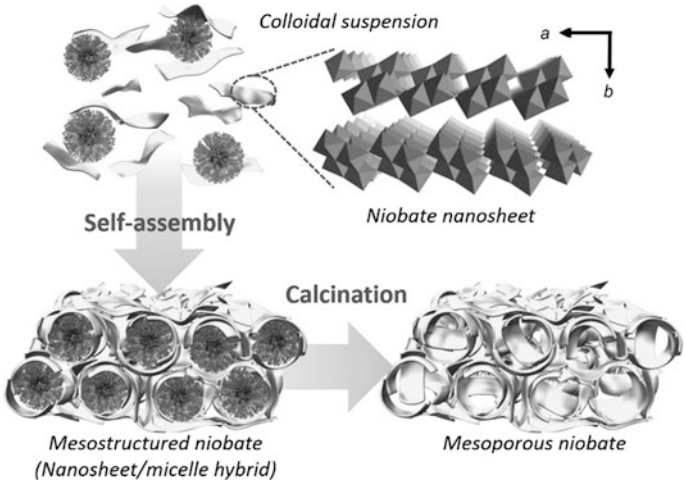

Fig. 3.24 Synthesis of crystalline mesoporous materials from coassembly of niobate nanosheets and polymeric micelles based on colloidal chemistry. Reprinted with permission from [277]. Copyright 2015 John Wiley & Sons, Inc

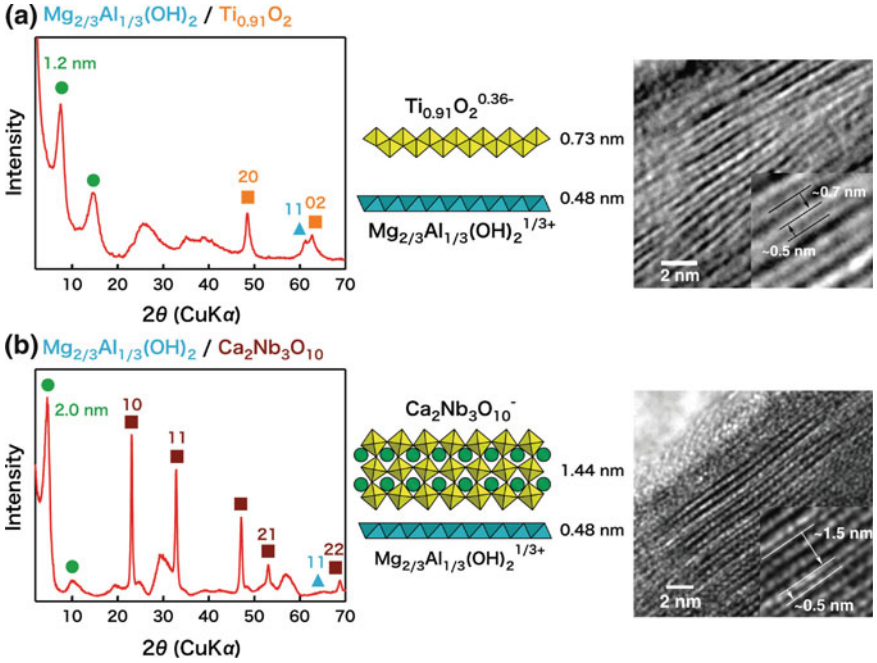

Fig. 3.25 XRD and TEM characterizations of the LDH/titanate or niobate nanosheet aggregates with alternately stacked layered structures. **a** $[Mg_{2/3}Al_{1/3}(OH)_2]^{1/3+}/Ti_{0.91}O_2{}^{0.36-}$ and B) $[Mg_{2/3}Al_{1/3}(OH)_2]^{1/3+}/Ca_2Nb_3O_{10}{}^{-}$. Reprinted with permission from [4]. Copyright 2010 John Wiley & Sons, Inc

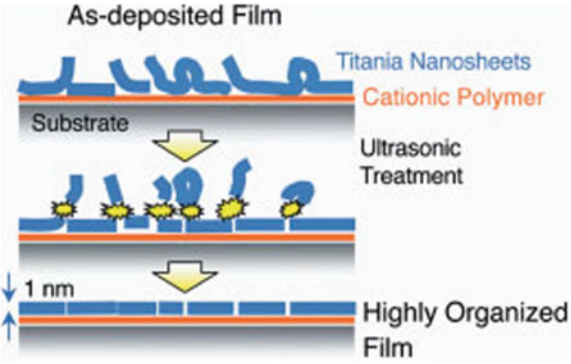

Fig. 3.26 Schematic illustration of the preparation of "perfect" cast film of lepidocrocite-type titanate nanosheets. Reprinted with permission from [286] (illustration of graphical abstract). Copyright 2004 John Wiley & Sons, Inc

have been used as electrodes and ion-exchangeable films. In these cast films, the deposited nanosheets are usually restacked to form layered structures that are disordered compared with the structures before exfoliation and often possess pores among the restacked nanosheets. Interstices and overlaps between the nanosheets are also usually unavoidable. These features facilitate molecular diffusion in the films, which is desirable for the electrochemical and ion-exchange processes. However, an almost "perfect" cast film with neat sheet tiling has been fabricated with lepidocrocite-type titanate nanosheets [286]. In this process, large nanosheets prepared from single crystals were deposited onto a substrate, which was modified in advance with cationic polymers in order to ensure the attachment of the negative nanosheets in a flat manner without interstices. Overlapping patches were then removed by ultrasonication (Fig. 3.26).

Nanosheet cast films are often prepared with ionic functional molecules, which can be incorporated in and/or adsorbed on the restacked nanosheets. The ionic molecules are immobilized through electrostatic interactions with the electrically charged nanosheets. Titanate nanosheets of $H_2Ti_3O_7$ exfoliated by PA^+ can regulate the orientation of cyanine dye molecules in their cast films [8]. When cast films of niobate nanosheets of $K_4Nb_6O_{17}$ exfoliated by triethanolammonium ions were soaked in an aqueous methylviologen (MV^{2+}) solution, photoinduced electron transfer occurred from the niobate nanosheets to the adsorbed MV^{2+} ions. The photochemical behavior was somewhat different from that observed for a conventional intercalation compound of the niobate and MV^{2+}, reflecting the difference in microenvironment of the MV^{2+} ions [102]. MV^{2+} has also been incorporated into an electrophoretically deposited titanate nanosheet film, and the film exhibited photoinduced electron transfer [287, 288]. Confinement of rare-earth cations in titanate and hydroxide nanosheet films through electrostatic self-assembly can provide specific microenvironments to realize photoluminescence of the rare-earth ions [289].

Hierarchically organized heterostructures consisting of titanate nanosheet cast films with immobilized MV^{2+} and mesoporous silica powders including porphyrin have been produced (Fig. 3.27) [290–292]. Upon visible-light excitation of the

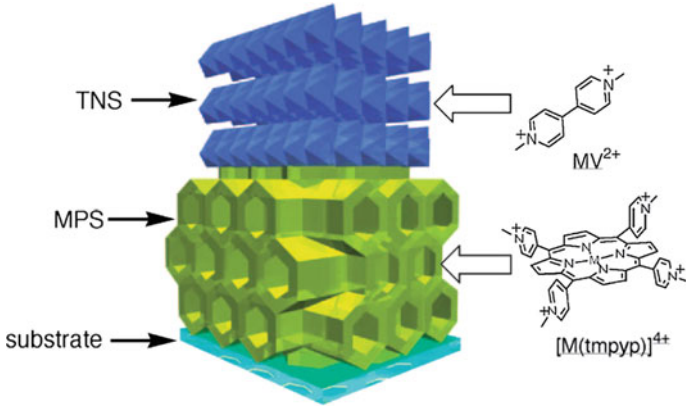

Fig. 3.27 Schematic structure of the [porphyrin–mesoporous silica (MPS)]/[MV^{2+}–titanate nanosheet (TNS)] hybrid films. Reprinted from [290]. Copyright 2006 The Chemical Society of Japan

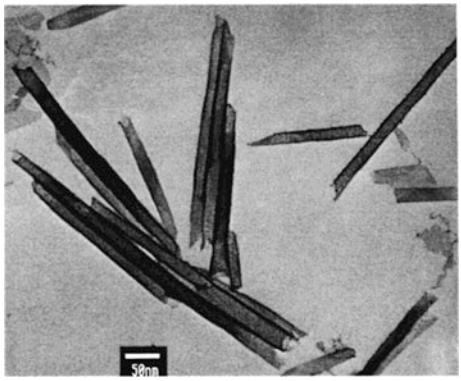

Fig. 3.28 TEM image of the niobate nanoscrolls of obtained from hexaniobate nanosheets. Reprinted with permission from [112]. Copyright 2000 American Chemical Society

porphyrin molecules, photoinduced electron transfer occurred from the porphyrin to MV^{2+} across the interface of the titanate nanosheets and mesoporous silica. A long-lived photoproduct was obtained by appropriate modification of the higher order structure.

3.6.1.3 Transformation to Nanoscrolls

Morphological transformation of nanosheets to nanoscrolls has been reported for nanosheets exfoliated from several cation-exchangeable layered solids. This transformation occurs by scrolling of the nanosheets into tubules. This phenomenon was discovered for niobate nanosheets obtained from $K_4Nb_6O_{17}$ (Fig. 3.28), and ascribed to their asymmetric surface structure given by the bilayer structure as

mentioned in Sect. 3.4.2 [112]. However, the scrolling has also been found for nanosheets exfoliated from other precursors such as lepidocrocite-type titanate, perovskite-type titanate and niobate, and manganate, which all form monolayer nanosheets [152, 293, 294].

The niobate nanoscrolls prepared from $K_4Nb_6O_{17}$ have been used as a 1D analog of the nanosheets. Their photo- and thermocatalytic properties have been examined in detail [10, 295–297]. In addition, incorporation of an azobenzene derivative (Azo) into niobate nanoscrolls has been investigated [298, 299]. In this system, cationic Azo molecules were intercalated into the scrolled nanosheets by cation exchange. The incorporated Azo molecules underwent photoisomerization, and their *trans–cis* transformation at the molecular level was magnified as sliding of the scrolled nanosheets, resulting in shape change at the micrometer-level.

It should be noted that all of the nanoscrolls mentioned above were identified only after the removal of solvents; clear evidence for scrolling of the nanosheets in the colloidal state has not been reported yet. This suggests that the nanosheets are scrolled as they dry, which is supported by the liquid crystallinity of the colloidal nanosheets. The liquid crystalline behavior of the niobate and titanate nanosheets is explained by individual nanosheets being well dispersed and retaining their 2D shape in the colloids [50, 300, 301]. Therefore, scrolling would occur during drying of the nanosheets. Removal of the solvent from the colloids concentrates coexisting electrolytes to facilitate aggregation of the nanosheets. This leads to wrinkling of the nanosheets and then the formation of nanoscrolls; thus, scrolling can be recognized as self-aggregation of nanosheets.

3.6.2 Layer-by-Layer Assemblies

LbL assembly is a technique used for fabricating multilayer thin films by repeated deposition of a monolayer onto a substrate. Although this method requires more elaborate operations than conventional film preparation techniques such as simple casting and spin-coating, LbL assembly is advantageous to precisely assemble thin films with defined nanostructures. Because the nanosheets exfoliated from ion-exchangeable layered solids bear electric charges, electrostatic sequential deposition, which is only called LbL assembly in a narrow sense, has been used more frequently for preparing thin films than the Langmuir–Blodgett (LB) method.

3.6.2.1 Electrostatic LbL Assemblies

This type of assemblies is obtained by alternating deposition of cationic and anionic monolayers onto a substrate [302, 303]. The first example of an electrostatic LbL assembly using exfoliated nanosheets was reported in 1984 for clay, α-ZrP, and niobate (from $K_4Nb_6O_{17}$) nanosheets [100, 304]. Film fabrication was initiated by grafting cationic groups onto a glass substrate. The substrate was soaked in an

aqueous colloidal suspension of nanosheets to deposit them on the substrate. Then, the substrate was withdrawn from the colloid, rinsed adequately, and transferred to an aqueous solution of polycations, such as poly(allylammonium), poly(diallyldimethylammonium), and polyethyeneimine, which caused the polymer countercations to adsorb on the nanosheets [305]. Multilayer films were fabricated by repeating the alternate deposition of nanosheets and polycations. Figure 3.29 illustrates the deposition process. Electrostatic LbL assembly has been rapidly extended to other electrically charged nanosheets such as titanates, manganates, and LDHs [28, 305, 306]. For the LbL assembly of LDH nanosheets, poly(styrene 4-sulfonate) has been used as a typical polymer counteranion. Inorganic clusters (e.g., $Al_{13}{}^{7+}$), biomacromolecules (e.g., cytochrome c), and nanoparticles can also be employed as the countercations [100, 307]. Alternating deposition of more than two kinds of the nanosheets such as cationic and anionic ones has yielded superstructured nanosheet multilayer films [251, 308, 309].

By appropriately combining nanosheets and counterions, the resulting nanosheet assemblies can show various functions. As an example, photoenergy conversion systems have been organized by assembling nanosheets and photofunctional molecules such as a sensitizers, electron/energy donors, and acceptors (Fig. 3.30) [12, 310]. Interlayer electron/energy transfer separated by the nanosheets has been identified. Use of the photocatalytically active semiconductor nanosheets, exemplified by titanates, enables their contribution to the photoprocesses [12, 311]. Photoinduced electron transfer between the electron-donating and -accepting nanosheets has been observed in a superstructured nanosheet film [308]. Meanwhile, LbL assembly of dielectric titanate and niobate nanosheets produces multilayer films with unusual electronic and magnetic properties, such as high-κ dielectric property [59–61, 87].

The LbL method is not limited to deposition on flat substrates. LbL fabrication of α-ZrP multilayer films on SiO_2 particles with polymer countercations was reported in 1995 [310]. In this system, by attaching photofunctional moieties such as photoseisitizing ruthenium-bipyridine and electron accepting viologen units to the polymer side chains, and by stacking the polymer layers to sandwich the α-ZrP nanosheets, photoinduced electron transfer occured in the multilayer films reflecting the stacking sequence of the polymer layers and nanosheets. The formation of nanosheet multilayers on PSt particles by LbL assembly gave materials with a core-shell structure [312–314]. These core-shell particles were converted to hollow capsules after removal of the PSt cores by calcination.

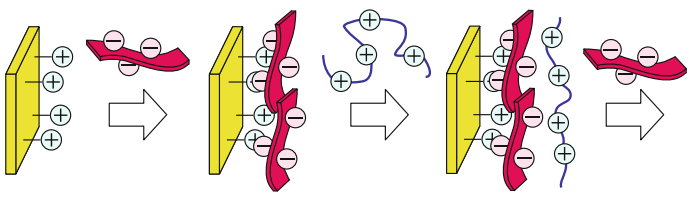

Fig. 3.29 Schematic illustration of the preparation of multilayer films through electrostatic LbL deposition of anionic nanosheets and cationic polymers

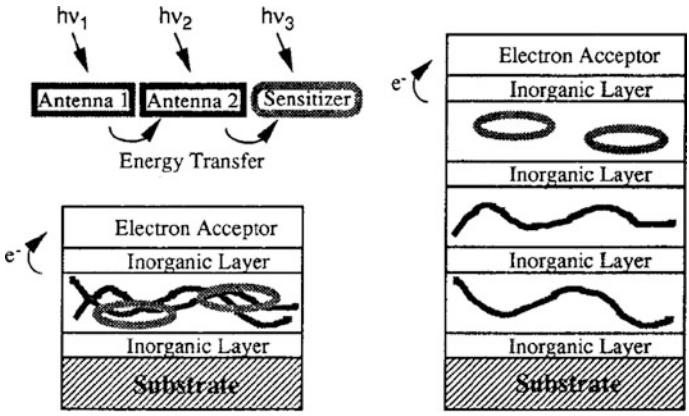

Fig. 3.30 Possible architectures for photoinduced intra- (*left*) and interlayer (*right*) energy transfer followed by interlayer electron transfer. Reprinted with permission from [12]. Copyright 119 American Chemical Society

3.6.2.2 Langmuir–Blodgett Films

The LB technique has also been used for fabricating inorganic nanosheet films although it is more complicated and time-consuming than electrostatic LbL deposition [315]. The LB method is advantageous to obtain high quality films with neat tiling. In fact, high-quality nanosheet multilayer films with few interstices and overlaps have been obtained with this technique [77]. LB films have been fabricated from the nanosheets of exfoliated layered titanates and niobates as well as clay minerals [77, 316–318]. Since these nanosheets are hydrophilic because of their layer charges, they are electrostatically attached by long-chain organic cations prior to LB casting (Fig. 3.31). By this treatment, they become located at the air–water interface and can be transferred onto a substrate at an appropriate surface pressure. Film deposition without the amphiphilic additives has also been achieved [77, 318].

Nanosheet LB films prepared from perovskite-type niobate $HSr_2Nb_3O_{10}$ displayed photoconductivity [80]. When a LB film deposited with long-chain alkylammonium ions was irradiated with UV light, the alkylammonium ions were decomposed by the photocatalytic activity of the niobate nanosheets, and then the film showed conductivity under the irradiation [156, 319]. Although LB films of nanosheets exfoliated from perovskite-type niobate ($HCa_2Nb_3O_{10}$) were paraelectric, they became ferroelectric when the perovskite nanosheets were appropriately superstructured with other niobate and titanate nanosheets [320].

3.6.2.3 Nanosheet Monolayer Films as Substrates for Crystal Growth

Nanosheet monolayer films deposited by the LB technique have been used as seed layers on which 3D crystals are grown with specific orientations. Thin films of

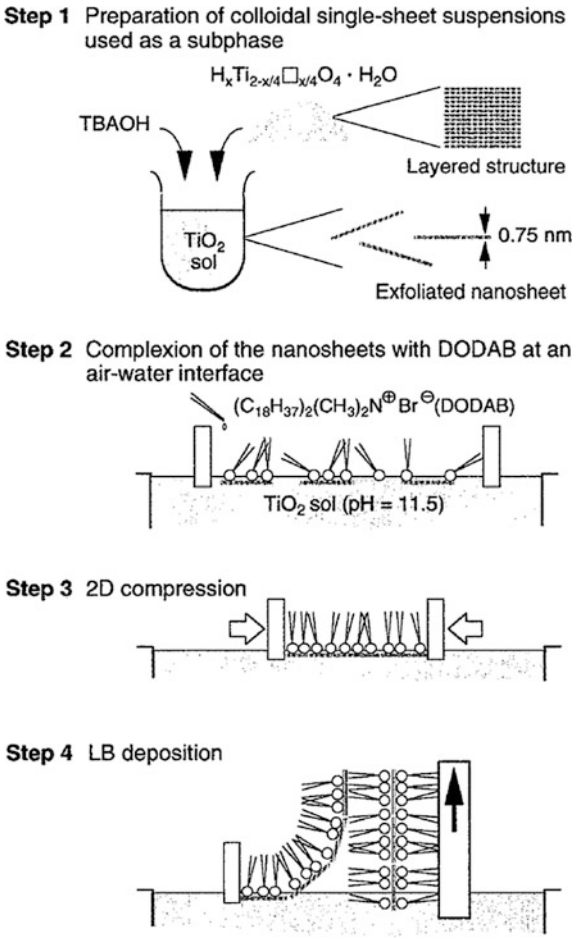

Fig. 3.31 Schematic illustration of the preparation process of the dioctadecyldimethylammonium bromide (DODAB)/titanate nanosheet alternating film using the LB technique. Reprinted with permission from [316]. Copyright 2001 American Chemical Society

cubic perovskites $SrTiO_3$ and $BaTiO_3$ have been epitaxially grown in the [100] direction on the LB monolayer perovskite-type niobate nanosheets exfoliated from $HCa_2Nb_3O_{10}$. Epitaxial growth was realized because of the crystallographic compatibility of the nanosheet surface and the (100) plane of the cubic perovskites (Fig. 3.32) [321–323]. LB monolayers of manganate and tungstate ($Cs_4W_{11}O_{36}$) nanosheets have been used for the growth of ZnO thin films in the [001] direction [321, 324].

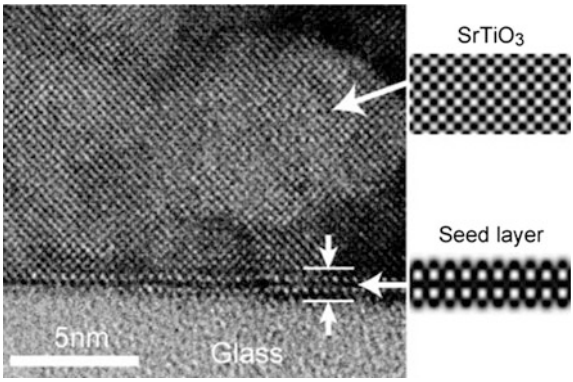

Fig. 3.32 Cross-sectional HRTEM image of an $SrTiO_3$ thin film on a nanosheet seed layer taken from the $SrTiO_3$ [100] direction. Reprinted with permission from [321]. Copyright 2004 John Wiley & Sons, Inc

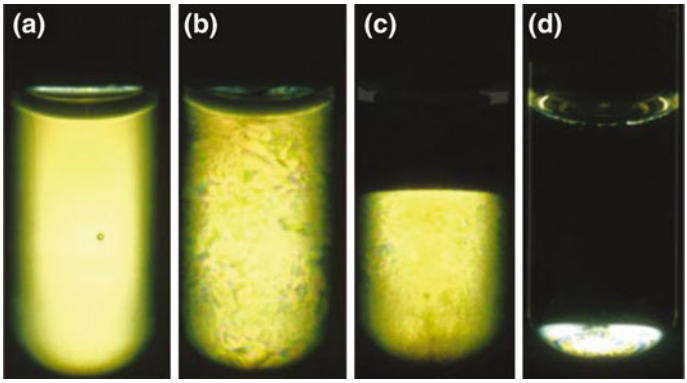

Fig. 3.33 Naked-eye observation of liquid crystalline nanosheet colloids of $H_3Sb_3P_2O_{14}$. Test-tubes filled with aqueous suspensions of the nanosheets, observed between crossed polarizers (**a**–**e**) (the isotropic phase in **c** and **d** appears dark). Reprinted with permission from [27]. Copyright 2001 Nature Publishing Group

3.6.3 Assemblies of the Nanosheets in the Colloidal State

Organization of nanosheets in the colloidal state yields characteristic assembled structures that are different from the bulk and LbL assemblies. A typical example is the liquid crystalline phase transition of the colloids (Fig. 3.33) [27, 325–328]. The liquid crystalline phases provide orientationally ordered structures of nanosheets in solvents, as described in Chap. 8. The fluid nature of the liquid crystalline phases enables macroscopic alignment of the colloidal nanosheets under external fields [325, 329, 330]. Another example is the sol–gel transition of colloidal nanosheets. While the exfoliated nanosheets are obtained as colloidal gels in some cases, a reversible sol–gel transition upon external pH stimuli has been reported for a colloid of niobate ($K_4Nb_6O_{17}$) nanosheets [331].

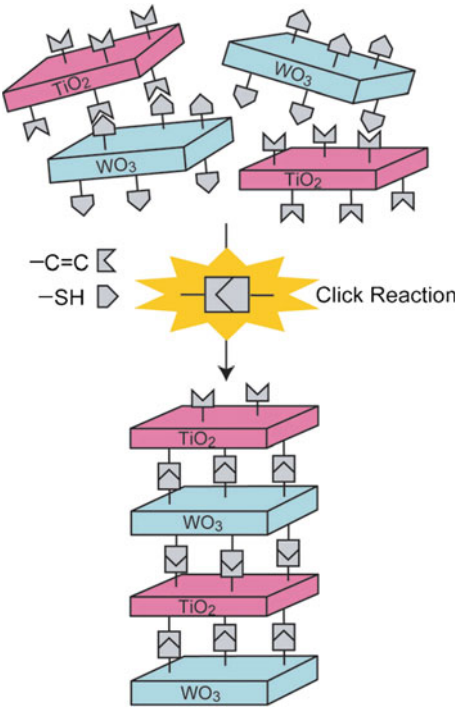

Fig. 3.34 Alternating layers of metal oxide obtained by a click reaction. Reprinted with permission from [332]. Copyright 2004 John Wiley & Sons, Inc

Controlled aggregation of the colloidal nanosheets can provide specifically organized nanosheets in the powder form. Alternate stacking of niobate/titanate (exfoliated from $K_4Nb_6O_{17}$ or $H_xTi_{2-x/4}\square_{x/4}O_4$, respectively) and tungstate (prepared from $H_2W_2O_7$) nanosheets has been attained through a thiol–ene click reaction (Fig. 3.34) [332, 333]. When niobate or titanate nanosheets with attached alkene moieties were mixed with tungstate nanosheets anchored by thiol groups, the click reaction proceeded between the niobate/titanate and tungstate nanosheets to bind them, resulting in the selective formation of a heterostructured product that was settled out from the colloid. Because the product consisted of two semiconducting oxides with different band positions, it realized efficient photoinduced electron transfer.

Emulsification of oil–water systems is also a promising way to assemble the colloidal nanosheets. Moderately hydrophobized solid particles are known to stabilize emulsions like organic surfactants. Such emulsions, called Pickering emulsions, have recently attracted attention because of their high stability and unusual properties induced by the particle emulsifiers [334, 335]. The emulsification induces particle aggregation at the oil–water interface. Ion-exchangeable layered crystals have also been examined as solid emulsifiers because their hydrophobicity can be modified by intercalation of organic molecules into the interlayer spaces or grafting them to the nanosheet surfaces. Although non-exfoliated layered crystals have been used in most cases [336–339], emulsification by α-ZrP and graphene

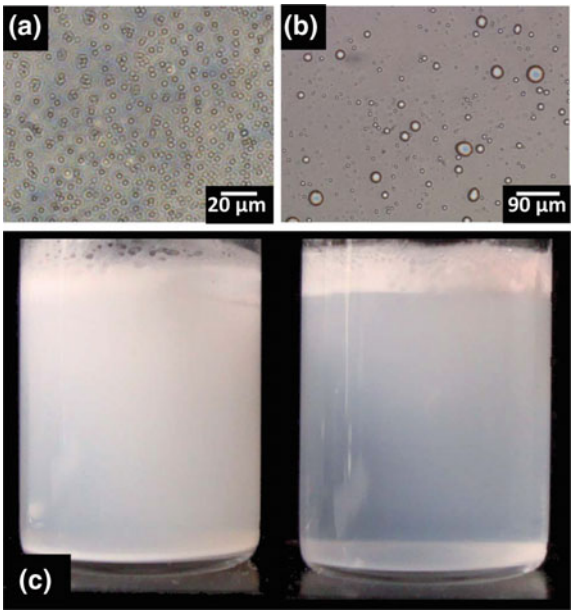

Fig. 3.35 Toluene-in-water emulsions stabilized by α-ZrP-ODI and nonmodified α-ZrP nano-sheets. **a** Micrograph of uniform toluene-in-water droplets stabilized by α-ZrP-ODI nano-sheets. **b** Micrograph of polydispersed toluene-in-water emulsion droplets stabilized by non-modified α-ZrP nano-sheets. **c** Toluene-in-water emulsions stabilized by non-modified α-ZrP (*right*) and stabilized by α-ZrP-ODI nano-sheets (*left*). Reprinted with permission from [341]. Copyright 2012 Royal Society of Chemistry

oxide nanosheets has recently been reported (Fig. 3.35) [340, 341]. This suggests the applicability of other exfoliated nanosheets as solid emulsifiers.

3.7 Summary and Outlook

Ion-exchangeable layered solids can be exfoliated by osmotic swelling with solvents; in most cases after displacing the interlayer ions for suitable ones called exfoliating reagents, which have an affinity for the employed solvent. There are a number of ion-exchangeable layered solids such as oxometallates, metal phosphates, and hydroxides, with a broad range of compositions. Thus, the inorganic nanosheets obtained through exfoliation possess diverse physicochemical functions based on their electric, magnetic, optic, photochemical, catalytic, and redox properties. The nanosheets can be assembled to form a variety of hierarchical structures; they are not limited to stacked films but can form porous solids, transformed structures such as nanoscrolls, and structured colloids. Many inorganic ion-exchangeable layered solids are still waiting for the development of exfoliation technology, and a much richer library of advanced materials based on exfoliated nanosheets should be established in the near future. In addition, combination of nanosheets with other building blocks with different structural motifs, such as porous powders, 0D and 1D particles, and biological macromolecules, will expand both the structural and functional variety of nanosheet-based materials.

References

1. van Olphen H (1991) Clay colloid chemistry (reprinted edition). Krieger, Malabar
2. Smalley M (2006) Clay swelling and colloid stability. Taylor & Francis, Boca Raton
3. Sasaki T (2007) J Ceram Soc Jpn 115:9
4. Ma R, Sasaki T (2010) Adv Mater 22:5082
5. Gunjakar JL, Kim IY, Lee JM, Jo YK, Hwang S-J (2014) J Phys Chem C 118:3847
6. Sasaki T, Watanabe M, Hashizume H, Yamada H, Nakazawa H (1996) Chem Commun 229
7. Harada M, Sasaki T, Ebina Y, Watanabe M (2002) J Photochem Photobiol, A 148:273
8. Miyamoto N, Kuroda K, Ogawa M (2004) J Mater Chem 14:165
9. Sugimoto W, Terabayashi O, Murakami Y, Takasu Y (2002) J Mater Chem 12:3814
10. Abe R, Shinohara K, Tanaka A, Hara M, Kondo JN, Domen K (1997) Chem Mater 9:2179
11. Nakato T, Miyamoto N, Harada A (2004) Chem Commun 78
12. Kaschak DM, Lean JT, Waraksa CC, Saupe GB, Usami H, Mallouk TE (1999) J Am Chem Soc 121:3435
13. Takagaki A, Yoshida T, Lu D, Kondo JN, Hara M, Domen K, Hayashi S (2004) J Phys Chem B 108:11549
14. Prasad G, Takei T, Arimoto K, Yonesaki Y, Kumada N, Kinomura N (2006) Solid State Ionics 177:197
15. Fukuda K, Nakai I, Ebina Y, Ma RZ, Sasaki T (2007) Inorg Chem 46:4787
16. Treacy MMJ, Rice SB, Jacobson AJ, Lewandowski JT (1990) Chem Mater 2:279
17. Tahara S, Takeda Y, Sugahara Y (2005) Chem Mater 17:6198
18. Schottenfeld JA, Kobayashi Y, Wang J, Macdonald DD, Mallouk TE (2008) Chem Mater 20:213
19. Liu Z-h, Ooi K, Kanoh H, Tang W-p, Tomida T (2000) Langmuir 16:4154
20. Kim TW, Oh E-J, Jee A-Y, Lim ST, Park DH, Lee M, Hyun S-H, Choy J-H, Hwang S-J (2009) Chem Eur J 15:10752
21. Sugimoto W, Iwata H, Yasunaga Y, Murakami Y, Takasu Y (2003) Angew Chem Int Ed 42:4092
22. Fukuda K, Saida T, Sato J, Yonezawa M, Takasu Y, Sugimoto W (2010) Inorg Chem 49:4391
23. Schaak RE, Mallouk TE (2002) Chem Commun 706
24. Fukuda K, Akatsuka K, Ebina Y, Ma R, Takada K, Nakai I, Sasaki T (2008) ACS Nano 2:1689
25. Ide Y, Ozaki G, Ogawa M (2009) Langmuir 25:5276
26. Alberti G, Casciola M, Costantino U (1985) J Colloid Interface Sci 107:256
27. Gabriel J-CP, Camerel F, Lemaire BJ, Desvaux H, Davidson P, Batail P (2001) Nature 413:504
28. Li L, Ma R, Ebina Y, Iyi N, Sasaki T (2005) Chem Mater 17:4386
29. Liu Z, Ma R, Osada M, Iyi N, Ebina Y, Takada K, Sasaki T (2006) J Am Chem Soc 128:4872
30. Demel J, Zhigunov A, Jirka I, Klementova M, Lang K (2015) J Colloid Interface Sci 452:174
31. Ida S, Sonoda Y, Ikeue K, Matsumoto Y (2010) Chem Commun 46:877
32. Raveau B (1984) Rev Chim Miner 21:391
33. Miyamoto N, Yamamoto H, Kaito R, Kuroda K (2002) Chem Commun 2378
34. Sasaki T, Watanabe M, Hashizume H, Yamada H, Nakazawa H (1996) J Am Chem Soc 118:8329
35. Sasaki T, Watanabe M (1998) J Am Chem Soc 120:4682
36. Geng F, Ma R, Nakamura A, Akatsuka K, Ebina Y, Yamauchi Y, Miyamoto N, Tateyama Y, Sasaki T (2013) Nat Commun 4:1632
37. Maluangnont T, Matsuba K, Geng F, Ma R, Yamauchi Y, Sasaki T (2013) Chem Mater 25:3137

38. Geng F, Ma R, Ebina Y, Yamauchi Y, Miyamoto N, Sasaki T (2014) J Am Chem Soc 136:5491
39. Geng F, Ma R, Yamauchi Y, Sasaki T (2014) Chem Commun 50:9977
40. Hervieu M, Raveau B (1981) Rev Chim Miner 18:642
41. Sasaki T, Watanabe M, Michiue Y, Komatsu Y, Izumi F, Takenouchi S (1995) Chem Mater 7:1001
42. Sasaki T, Izumi F, Watanabe M (1996) Chem Mater 8:777
43. Barbier G (1934) Compt Rend 199:226
44. Ebina Y, Sasaki T, Watanabe M (2002) Solid State Ionics 151:177
45. Omomo Y, Sasaki T, Wang L, Watanabe M (2003) J Am Chem Soc 125:3568
46. Ohya T, Nakayama A, Takahasbi B, Ohya Y, Takahashi Y (2002) Chem Mater 14:3082
47. Kamada K, Soh N (2014) RSC Adv 4:8682
48. Tanaka T, Ebina Y, Takada K, Kurashima K, Sasaki T (2003) Chem Mater 15:3564
49. O'Neill A, Khan U, Coleman JN (2012) Chem Mater 24:2414
50. Miyamoto N, Nakato T (2004) J Phys Chem B 108:6152
51. Wang L, Sasaki T (2014) Chem Rev 114:9455
52. Le Granvalet-Mancini M, Brohan L, Marie A-M, Tournoux M (1994) Eur J Solid State Inorg Chem 31:767
53. Ide Y, Sadakane M, Sano T, Ogawa M (2014) J Nanosci Nanotechnol 14:2135
54. Fujiki Y, Komatsu Y, Ohta N (1980) Chem Lett 1023
55. Izawa H, Kikkawa S, Koizumi M (1982) J Phys Chem 86:5023
56. Clément P, Marchand R (1983) C R Acad Sci Paris II(296):1161
57. Izawa H, Kikkawa S, Koizumi M (1983) Polyhedron 2:741
58. Sasaki T, Watanabe M, Komatsu Y, Fujiki Y (1985) Inorg Chem 24:2265
59. Osada M, Ebina Y, Takada K, Sasaki T (2006) Adv Mater 18:295
60. Osada M, Ebina Y, Fukuda K, Ono K, Takada K, Yamaura K, Takayama-Muromachi E, Sasaki T (2006) Phys Rev B 73:153301
61. Osada M, Itose M, Ebina Y, Ono K, Ueda S, Kobayashi K, Sasaki T (2008) Appl Phys Lett 92:253110
62. Dong XP, Osada M, Ueda H, Ebina Y, Kotani Y, Ono K, Ueda S, Kobayashi K, Takada K, Sasaki T (2009) Chem Mater 21:4366
63. Gao T, Fjellvåg H, Norby P (2009) J Mater Chem 19:787
64. Berry KL, Aftandilian VD, Gilbert WW, Meibohm EPH, Young HS (1960) J Inorg Nucl Chem 14:231
65. Andersson S (1961) Acta Crystallogr 14:1245
66. Besselink R, Stawski TM, Castricum HL, Blank DHA, ten Elshof JE (2010) J Phys Chem C 114:21281
67. Wang Y, Sun C, Yan X, Xiu F, Wang L, Smith SC, Wang KL, Lu GQ, Zou J (2011) J Am Chem Soc 133:695
68. Sugimoto W, Ohuchi K, Murakami Y, Takasu Y (2005) Bull Chem Soc Jpn 78:633
69. Ide Y, Ogawa M (2005) Chem Lett 34:360
70. Ide Y, Ogawa M (2006) J Colloid Interface Sci 296:141
71. Honda M, Oaki Y, Imai H (2014) Chem Mater 26:3579
72. Shibata M, Kudo A, Tanaka A, Domen K, Maruya K, Onishi T (1987) Chem Lett 1017
73. Miyata H, Sugahara Y, Kuroda K, Kato C (1988) J Chem Soc, Faraday Trans 1(84):2677
74. Nakato T, Kuroda K (1995) Eur J Solid State Inorg Chem 32:809
75. Domen K, Kondo JN, Hara M, Takata T (2000) Bull Chem Soc Jpn 73:1307
76. Osterloh FE (2008) Chem Mater 20:35
77. Akatsuka K, Haga M, Ebina Y, Osada M, Fukuda K, Sasaki T (2009) ACS Nano 3:1097
78. Osada M, Sasaki T (2012) Adv Mater 24:210
79. Choy J-H, Lee H-C, Jung H, Kim H, Boo H (2002) Chem Mater 14:2486
80. Umemura Y, Shinohara E, Koura A, Nishioka T, Sasaki T (2006) Langmuir 22:3870
81. Shibata T, Sakai N, Fukuda K, Ebina Y, Sasaki T (2007) Phys Chem Chem Phys 9:2413
82. Matsumoto Y, Ida S, Inoue T (2008) J Phys Chem C 112:11614

83. Allen MR, Thibert A, Sabio EM, Browning ND, Larsen DS, Osterloh FE (2010) Chem Mater 22:1220
84. Jo YK, Kim IY, Gunjakar JL, Lee JM, Lee NS, Lee SH, Hwang SJ (2014) Chem Eur J 20:10011
85. Liu G, Wang LZ, Sun CH, Chen ZG, Yan XX, Cheng L, Cheng HM, Lu GQ (2009) Chem Commun 1383
86. Liu G, Sun C, Wang L, Smith SC, Lu GQ, Cheng H-M (2011) J Mater Chem 21:14672
87. Osada M, Takanashi G, Li B-W, Akatsuka K, Ebina Y, Ono K, Funakubo H, Takada K, Sasaki T (2011) Adv Funct Mater 21:3482
88. Osada M, Sasaki T, Ono K, Kotani Y, Ueda S, Kobayashi K (2011) ACS Nano 5:6871
89. Bizeto MA, Shiguihara AL, Constantino VRL (2009) J Mater Chem 19:2512
90. Lagaly G, Beneke K (1976) J Inorg Nucl Chem 38:1513
91. Gasperin M, Le Bihan MT (1982) J Solid State Chem 43:346
92. Gasperin M (1982) Acta Cryst. B 38:2024
93. Nedjar R, Borel MM, Raveau B (1985) Mater Res Bull 20:1291
94. Wadsley AD (1964) Acta Cryst 17:623
95. Blasse G, de Pauw ADM (1970) J Inorg Nucl Chem 32:3960
96. Rebbah H, Borel MM, Raveau B (1980) Mater Res Bull 15:317
97. Rebbah H, Hervieu M, Raveau B (1981) Mater Res Bull 16:149
98. Bhat V, Gopalakrishnan J (1988) Solid State Ionics 26:25
99. Song H, Sjåstad AO, Fjellvåg H, Okamoto H, Vistad ØB, Arstad B, Norby P (2011) J Solid State Chem 184:3135
100. Keller SW, Kim H-N, Mallouk TE (1994) J Am Chem Soc 116:8817
101. Du GH, Yu Y, Chen Q, Wang RH, Zhou W, Peng LM (2003) Chem Phys Lett 377:445
102. Nakato T, Edakubo H, Shimomura T (2009) Micropor Mesopor Mater 123:280
103. Park I, Han YS, Choy JH (2009) J Nanosci Nanotechnol 9:7190
104. Galasso F, Darby W (1962) J Phys Chem 66:1318
105. Toda K, Tokuoka S, Uematsu K, Sato M (2002) Key Eng Mater 214–215:67
106. Toda K, Ohtake N, Kawakami M, Tokuoka S, Uematsu K, Sato M (2002) Jpn J Appl Phys 41:7021
107. Tagusagawa C, Takagaki A, Hayash S, Domen K (2009) J Phys Chem C 113:7831
108. Kinomura N, Kumada N, Muto F (1985) J Chem Soc, Dalton Trans 2349
109. Nakato T, Sakamoto D, Kuroda K, Kato C (1992) Bull Chem Soc Jpn 65:322
110. Nakato T, Miyamoto N (2002) J Mater Chem 12:1245
111. Miyamoto N, Nakato T (2003) Langmuir 19:8057
112. Saupe GB, Waraksa CC, Kim H-N, Han YJ, Kaschak DM, Skinner DM, Mallouk TE (2000) Chem Mater 12:1556
113. Bizeto MA, Constantino VRL (2004) Mater Res Bull 39:1811
114. Nakato T, Hashimoto S (2007) Chem Lett 36:1240
115. Kimura N, Kato Y, Suzuki R, Shimada A, Tahara S, Nakato T, Matsukawa K, Mutin PH, Sugahara Y (2014) Langmuir 30:1169
116. Miyamoto N, Yamada Y, Koizumi S, Nakato T (2007) Angew Chem Int Ed 46:4123
117. Usami H, Nakamura T, Makino T, Fujimatsu H, Ogasawara S (1998) J Chem Soc, Faraday Trans 94:83
118. Sarahan MC, Carroll EC, Allen M, Larsen DS, Browning ND, Osterloh FE (2008) J Solid State Chem 181:1678
119. Huang J, Ma R, Ebina Y, Fukuda K, Takada K, Sasaki T (2010) Chem Mater 22:2582
120. Shibata T, Takanashi G, Nakamura T, Fukuda K, Ebina Y, Sasaki T (2011) Energy Environ Sci 4:535
121. Liang S, Wen L, Lin S, Bi J, Feng P, Fu X, Wu L (2014) Angew Chem Int Ed Engl 53:2951
122. Nakato T, Fujita T, Mouri E (2015) Phys Chem Chem Phys 17:5547
123. Yin G, Nishikawa M, Nosaka Y, Srinivasan N, Atarashi D, Sakai E, Miyauchi M (2015) ACS Nano 9:2111

124. Liu Y, Xiong J, Luo S, Liang R, Qin N, Liang S, Wu L (2015) Chem Commun (Camb) 51:15125
125. Xiong J, Wen L, Jiang F, Liu Y, Liang S, Wu L (2015) J Mater Chem A 3:20627
126. Koinuma M, Seki H, Matsumoto Y (2002) J Electroanal Chem 531:81
127. Akatsuka K, Takanashi G, Ebina Y, Sakai N, Haga M, Sasaki T (2008) J Phys Chem Solids 69:1288
128. Akatsuka K, Takanashi G, Ebina Y, Haga M-a, Sasaki T (2012) J Phys Chem C 116:12426
129. Takagaki A, Sugisawa M, Lu D, Kondo JN, Hara M, Domen K, Hayashi S (2003) J Am Chem Soc 125:5479
130. Takagaki A, Lu D, Kondo JN, Hara M, Hayashi S, Domen K (2005) Chem Mater 17:2487
131. Schaak RE, Mallouk TE (2002) Chem Mater 14:1455
132. Ranmohotti KG, Josepha E, Choi J, Zhang J, Wiley JB (2011) Adv Mater 23:442
133. Dion M, Ganne M, Tournoux M (1981) Mater Res Bull 16:1429
134. Jacobson AJ, Johnson JW, Lewandowski JT (1985) Inorg Chem 24:3727
135. Ruddlesden SN, Popper P (1957) Acta Crystallogr 10:538
136. Ruddlesden SN, Popper P (1958) Acta Crystallogr 11:54
137. Gopalakrishnan J, Bhat V (1987) Inorg Chem 26:4299
138. Gopalakrishnan J, Bhat V, Raveau B (1987) Mater Res Bull 22:413
139. Tahara S, Ichikawa T, Kajiwara G, Sugahara Y (2007) Chem Mater 19:2352
140. Schaak RE, Mallouk TE (2000) Chem Mater 12:2513
141. Han Y-S, Park I, Choy J-H (2001) J Mater Chem 11:1277
142. Xu FF, Ebina Y, Bando Y, Sasaki T (2003) J Phys Chem B 107:9638
143. Gao H, Shori S, Chen X, zur Loye HC, Ploehn HJ (2013) J Colloid Interface Sci 392:226
144. Ozawa TC, Fukuda K, Akatsuka K, Ebina Y, Sasaki T (2007) Chem Mater 19:6575
145. Ida S, Ogata C, Eguchi M, Youngblood WJ, Mallouk TE, Matsumoto Y (2008) J Am Chem Soc 130:7052
146. Ozawa TC, Fukuda K, Akatsuka K, Ebina Y, Sasaki T, Kurashima K, Kosuda K (2008) J Phys Chem C 112:17115
147. Ozawa TC, Fukuda K, Akatsuka K, Ebina Y, Kurashima K, Sasaki T (2009) J Phys Chem C 113:8735
148. Ebina Y, Akatsuka K, Fukuda K, Sasaki T (2012) Chem Mater 24:4201
149. Ozawa TC, Fukuda K, Ebina Y, Sasaki T (2013) Inorg Chem 52:415
150. Ozawa TC, Onoda M, Iyi N, Ebina Y, Sasaki T (2014) J Phys Chem C 118:1729
151. Ida S, Okamoto Y, Matsuka M, Hagiwara H, Ishihara T (2012) J Am Chem Soc 134:15773
152. Schaak RE, Mallouk TE (2000) Chem Mater 12:3427
153. Ida S, Ogata C, Unal U, Izawa K, Inoue T, Altuntasoglu O, Matsumoto Y (2007) J Am Chem Soc 129:8956
154. Inaba K, Suzuki S, Noguchi Y, Miyayama M, Toda K, Sato M (2008) Eur J Inorg Chem 2008:5471
155. Kim J-Y, Chung I, Choy J-H, Park G-S (2001) Chem Mater 13:2759
156. Saruwatari K, Sato H, Kameda J, Yamagishi A, Domen K (2005) Chem Commun 1999
157. Ebina Y, Sakai N, Sasaki T (2005) J Phys Chem B 109:17212
158. Izawa K, Yamada T, Unal U, Ida S, Altuntasoglu O, Koinuma M, Matsumoto Y (2006) J Phys Chem B 110:4645
159. Okamoto K, Sato H, Saruwatari K, Tamura K, Kameda J, Kogure T, Umemura Y, Yamagishi A (2007) J Phys Chem C 111:12827
160. Sato H, Okamoto K, Tamura K, Yamada H, Saruwatari K, Kogure T, Yamagishi A (2008) Appl Phys Exp 1:0355001
161. Sabio EM, Chi M, Browning ND, Osterloh FE (2010) Langmuir 26:7254
162. Compton OC, Carroll EC, Kim JY, Larsen DS, Osterloh FE (2007) J Phys Chem C 111:14589
163. Compton OC, Osterloh FE (2009) J Phys Chem C 113:479
164. Sabio EM, Chamousis RL, Browning ND, Osterloh FE (2012) J Phys Chem C 116:3161
165. Maeda K, Eguchi M, Oshima T (2014) Angew Chem Int Ed 53:13164

166. Oshima T, Lu D, Ishitani O, Maeda K (2015) Angew Chem Int Ed Engl 54:2698
167. Li BW, Osada M, Ebina Y, Akatsuka K, Fukuda K, Sasaki T (2014) ACS Nano 8:5449
168. Wang CX, Osada M, Ebina Y, Li BW, Akatsuka K, Fukuda K, Sugimoto W, Ma RZ, Sasaki T (2014) ACS Nano 8:2658
169. Osada M, Akatsuka K, Ebina Y, Funakubo H, Ono K, Takada K, Sasaki T (2010) ACS Nano 4:5225
170. Feng Q, Kanoh H, Ooi K (1999) J Mater Chem 9:319
171. Giovanoli R, Staehli E, Feitknecht W (1970) Helv Chim Acta 53:209
172. Golden DC, Dixon JB, Chen CC (1986) Clays Clay Miner 34:511
173. Liu ZH, Yang XJ, Makita Y, Ooi K (2002) Chem Mater 14:4800
174. Fukuda K, Nakai I, Ebina Y, Tanaka M, Mori T, Sasaki T (2006) J Phys Chem B 110:17070
175. Borgohain R, Selegue JP, Cheng YT (2014) J Mater Chem A 2:20367
176. Kai K, Yoshida Y, Kageyama H, Saito G, Ishigaki T, Furukawa Y, Kawamata J (2008) J Am Chem Soc 130:15938
177. Kang J-H, Paek S-M, Hwang S-J, Choy J-H (2010) J Mater Chem 20:2033
178. Song MS, Lee KM, Lee YR, Kim IY, Kim TW, Gunjakar JL, Hwang SJ (2010) J Phys Chem C 114:22134
179. Mizushima K, Jones PC, Wiseman PJ, Goodenough JB (1980) Mater Res Bull 15:783
180. Alcántara R, Lavela P, Tirado JL, Zhecheva E, Stoyanova R (1999) J Solid State Electrochem 3:121
181. Whittingham MS (2004) Chem Rev 104:4271
182. Johnston WD, Heikes RR, Sestrich D (1958) J Phys Chem Solids 7:1
183. Kim J-Y, Kim J-I, Choi S-M, Soo Lim Y, Seo W-S, Hwang HJ (2012) J Appl Phys 112:113705
184. Carewska M, Scaccia S, Croce F, Arumugam S, Wang Y, Greenbaum S (1997) Solid State Ionics 93:227
185. Aksit M, Toledo DP, Robinson RD (2012) J Mater Chem 22:5936
186. Conway BE (1999) Electrochemical supercapacitors: scientific fundamentals and technological applications. Plenum Press, New York
187. Schwieger W, Lagaly G (2004) In: Auerbach SM, Carrado KA, Dutta PK (eds) Handbook of layered materials. Marcel Dekker, New York
188. Takahashi N, Kuroda K (2011) J Mater Chem 21:14336
189. Selvam T, Inayat A, Schwieger W (2014) Dalton Trans 43:10365
190. Colville AA, Anderson CP, Black PM (1971) Am Mineral 56:1220
191. Vortmann S, Rius J, Marler B, Gies H (1999) Eur J Mineral 11:125
192. Vortmann S, Rius J, Siegmann S (1997) J Phys Chem B 101:1292
193. Brandt A, Schwieger W, Bergk K-H (1987) Rev Chim Miner 24:564
194. Takahashi N, Hata H, Kuroda K (2011) Chem Mater 23:266
195. Boucher MA, Katsoulis DE, Kenney ME (2006) Chem Mater 18:360
196. Clearfield A, Smith DG (1969) Inorg Chem 8:431
197. Alberti G, Costantino U (1982) In: Whittingham MS, Jacobson AJ (eds) Intercalation chemistry. Academic Press, New York
198. Kumar CV, Bhambhani A, Hnatiuk N (2004) In: Auerbach SM, Carrado KA, Dutta PK (eds) Handbook of layered materials. Marcel Dekker, New York
199. Whittingham MS, Jacobson AJ (eds) (1982) Intercalation chemistry. Academic Press, New York
200. Wong M, Ishige R, Hoshino T, Hawkins S, Li P, Takahara A, Sue H-J (2014) Chem Mater 26:1528
201. Alberti G, Cavalaglio S, Dionigi C, Marmottini F (2000) Langmuir 16:7663
202. Casciola M, Alberti G, Donnadio A, Pica M, Marmottini F, Bottino A, Piaggio P (2005) J Mater Chem 15:4262
203. Piffard Y, Verbaere A, Lachgar A, Deniard-Courant S, Tournoux M (1987) Rev Chim Miner 23:766
204. Huang Q, Wang W, Yue Y, Hua W, Gao Z (2003) J Colloid Interface Sci 257:268

205. Tanaka H, Okumiya T, S-k Ueda, Taketani Y, Murakami M (2009) Mater. Res Bull 44:328
206. Takei T, Yonesaki Y, Kumada N, Kinomura N (2008) Langmuir 24:8554
207. Kalousová J, Votinský J, Beneš L, Melánová K, Zima V (1998) Collect Czech Chem Commun 63:1
208. Nakato T, Furumi Y, Okuhara T (1998) Chem Lett 611
209. Yamamoto N, Okuhara T, Nakato T (2001) J Mater Chem 11:1858
210. Choy JH, Kwon SJ, Hwang SJ, Kim YI, Lee W (1999) J Mater Chem 9:129
211. Jang ES, Chang JJ, Jeon SH, Khim ZG, Choy JH (2005) Adv Mater 17:1742
212. Kim DS, Ozawa TC, Fukuda K, Ohshima S, Nakai I, Sasaki T (2011) Chem Mater 23:2700
213. Weiss A, Sick E (1978) Z Naturforsch 33b:1087
214. Lévy FA (ed) (1979) Intercalated layered materials. D. Reidel, Dordrecht
215. Lerf A, Schöllhorn R (1977) Inorg Chem 16:2950
216. Frondel C (1941) Am Mineral 26:295
217. Feitknecht W (1942) Helv Chim Acta 25:555
218. Miyata S (1983) Clays Clay Miner 31:305
219. Taylor RM (1984) Clay Miner 19:591
220. Reichle WT (1986) ChemTech 16:58
221. Duan X, Evans DG (2005) Layered double hydroxides. Springer, Berlin, New York
222. Khan AI, O'Hare D (2002) J Mater Chem 12:3191
223. Leroux F, Taviot-Gueho C (2005) J Mater Chem 15:3628
224. Williams GR, O'Hare D (2006) J Mater Chem 16:3065
225. Debecker DP, Gaigneaux EM, Busca G (2009) Chem Eur J 15:3920
226. Wang Q, O'Hare D (2012) Chem Rev 112:4124
227. Adachi-Pagano M, Forano C, Besse JP (2000) Chem Commun 91
228. Ma R, Liu Z, Li L, Iyi N, Sasaki T (2006) J Mater Chem 16:3809
229. Wu Q, Olafsen A, Vistad ØB, Roots J, Norby P (2005) J Mater Chem 15:4695
230. Ma R, Liu Z, Takada K, Iyi N, Bando Y, Sasaki T (2007) J Am Chem Soc 129:5257
231. O'Leary S, O'Hare D, Seeley G (2002) Chem Commun 1506
232. Singh M, Ogden MI, Parkinson GM, Buckley CE, Connolly J (2004) J Mater Chem 14:871
233. Jobbagy M, Regazzoni AE (2004) J Colloid Interface Sci 275:345
234. Naik VV, Ramesh TN, Vasudevan S (2011) J Phys Chem Lett 2:1193
235. Naik VV, Vasudevan S (2011) Langmuir 27:13276
236. Wang Q, O'Hare D (2013) Chem Commun 49:6301
237. Hibino T, Kobayashi M (2005) J Mater Chem 15:653
238. Jaubertie C, Holgado MJ, San Roman MS, Rives V (2006) Chem Mater 18:3114
239. Hou W, Kang L, Sun R, Liu Z-H (2008) Colloids Surf A 312:92
240. Manohara GV, Kunz DA, Kamath PV, Milius W, Breu J (2010) Langmuir 26:15586
241. Gardner E, Huntoon KM, Pinnavaia TJ (2001) Adv Mater 13:1263
242. Iyi N, Ishihara S, Kaneko Y, Yamada H (2013) Langmuir 29:2562
243. Wang Y, Yang W, Chen C, Evans DG (2008) J Power Sources 184:682
244. Latorre-Sanchez M, Atienzar P, Abellán G, Puche M, Fornés V, Ribera A, García H (2012) Carbon 50:518
245. Lee JM, Gunjakar JL, Ham Y, Kim IY, Domen K, Hwang SJ (2014) Chem Eur J 20:17004
246. Liang YN, Li Y, Ang C, Shen Y, Chi D, Hu X (2014) ACS Appl Mater Interfaces 6:12406
247. Lee JH, Chang J, Cha JH, Jung DY, Kim SS, Kim JM (2010) Chem Eur J 16:8296
248. Yan D, Qin S, Chen L, Lu J, Ma J, Wei M, Evans DG, Duan X (2010) Chem Commun 46:8654
249. Yan D, Lu J, Ma J, Wei M, Evans DG, Duan X (2011) Angew Chem Int Ed 50:720
250. Yan D, Lu J, Ma J, Qin S, Wei M, Evans DG, Duan X (2011) Angew Chem Int Ed 50:7037
251. Li L, Ma RZ, Ebina Y, Fukuda K, Takada K, Sasaki T (2007) J Am Chem Soc 129:8000
252. Deák Á, Janovák L, Tallósy SP, Bitó T, Sebők D, Buzás N, Pálinko I, Dékány I (2015) Langmuir 31:2019
253. Xu ZP, Niebert M, Porazik K, Walker TL, Cooper HM, Middelberg AP, Gray PP, Bartlett PF, Lu GQ (2008) J Control Release 130:86

254. An Z, Lu S, He J, Wang Y (2009) Langmuir 25:10704
255. Park DH, Kim JE, Oh JM, Shul YG, Choy JH (2010) J Am Chem Soc 132:16735
256. Playle AC, Gunning SR, Llewellyn AF (1974) Pharm Acta Helv 49:298
257. Costantino U, Ambrogi V, Nocchetti M, Perioli L (2008) Micropor. Mesopor. Mater. 107:149
258. Hawthorne FC (1985) Mineral Mag 49:87
259. Yamanaka S, Sako T, Seki K, Hattori M (1992) Solid State Ionics 53–56:527
260. Backov R, Morga AN, Lane S, Perez-Cordero EE, Williams K, Meisel MW, Sanchez C, Talham DR (2002) Mol Cryst Liq Cryst 376:127
261. Miao JY, Xue M, Itoh H, Feng Q (2006) J Mater Chem 16:474
262. Haschke JM (1974) Inorg Chem 13:1812
263. Louer D, Louer M (1987) J Solid State Chem 68:292
264. Geng FX, Xin H, Matsushita Y, Ma RZ, Tanaka M, Izumi F, Iyi N, Sasaki T (2008) Chem Eur J 14:9255
265. McIntyre LJ, Jackson LK, Fogg AM (2008) Chem Mater 20:335
266. Lee K-H, Byeon S-H (2009) Eur J Inorg Chem 2009:929
267. Hu L, Ma R, Ozawa TC, Sasaki T (2010) Chem Asian J 5:248
268. Sasaki T, Nakano S, Yamauchi S, Watanabe M (1997) Chem Mater 9:602
269. Ebina Y, Sasaki T, Harada M, Watanabe M (2002) Chem Mater 14:4390
270. Zhou Y, Huang R, Ding F, Brittain AD, Liu J, Zhang M, Xiao M, Meng Y, Sun L (2014) ACS Appl Mater Interfaces 6:7417
271. Kooli F, Sasaki T, Watanabe M (1999) Micropor Mesopor Mater 28:495
272. Wang LZ, Ebina Y, Takada K, Kurashima K, Sasaki T (2004) Adv Mater 16:1412
273. Kim TW, Hur SG, Hwang S-J, Choy J-H (2006) Chem Commun 220
274. Kim TW, Hur SG, Hwang SJ, Park H, Choi W, Choy JH (2007) Adv Funct Mater 17:307
275. Hata H, Kobayashi Y, Bojan V, Youngblood WJ, Mallouk TE (2008) Nano Lett 8:794
276. Miyamoto N, Kuroda K (2007) J Colloid Interface Sci 313:369
277. Bastakoti BP, Li Y, Imura M, Miyamoto N, Nakato T, Sasaki T, Yamauchi Y (2015) Angew Chem Int Ed Engl 54:4222
278. Hu Q, Xu Z, Qiao S, Haghseresht F, Wilson M, Lu GQ (2007) J Colloid Interface Sci 308:191
279. Kamada K, Tsukahara S, Soh N (2011) J Phys Chem C 115:13232
280. Tsukahara S, Soh N, Kamada K (2012) J Phys Chem C 116:19285
281. Sumida T, Takahara Y, Abe R, Hara M, Kondo JN, Domen K, Kakihana M, Yoshimura M (2001) Phys Chem Chem Phys 3:640
282. Wang L, Takada K, Kajiyama A, Onoda M, Michiue Y, Zhang L, Watanabe M, Sasaki T (2003) Chem Mater 15:4508
283. Okamoto K, Sasaki T, Fujita T, Iyi N (2006) J Mater Chem 16:1608
284. Suzuki S, Miyayama M (2006) J Phys Chem B 110:4731
285. Matsuda A, Sakamoto H, Mohd Nor MA, Kawamura G, Muto H (2013) J Phys Chem B 117:1724
286. Tanaka T, Fukuda K, Ebina Y, Takada K, Sasaki T (2004) Adv Mater 16:872
287. Yui T, Mori Y, Tsuchino T, Itoh T, Hattori T, Fukushima Y, Takagi K (2005) Chem Mater 17:206
288. Matsumoto Y, Unal U, Kimura Y, Ohashi S, Izawa K (2005) J Phys Chem B 109:12748
289. Lee KH, Lee BI, You JH, Byeon SH (2010) Chem Commun 46:1461
290. Yui T, Tsuchino T, Akatsuka K, Yamauchi A, Kobayashi Y, Hattori T, M-a Haga, Takagi K (2006) Bull Chem Soc Jpn 79:386
291. Yui T, Tsuchino T, Itoh T, Ogawa M, Fukushima Y, Takagi K (2005) Langmuir 21:2644
292. Yui T, Kobayashi Y, Yamada Y, Yano K, Fukushima Y, Torimoto T, Takagi K (2011) ACS Appl Mater Interfaces 3:931
293. Ma RZ, Bando Y, Sasaki T (2004) J Phys Chem B 108:2115
294. Kobayashi Y, Hata H, Salama M, Mallouk TE (2007) Nano Lett 7:2142

295. Bizeto MA, Alves WA, Barbosa CAS, Ferreira AMDC, Constantino VRL (2006) Inorg Chem 45:6214
296. Ma R, Kobayashi Y, Youngblood WJ, Mallouk TE (2008) J Mater Chem 18:5982
297. Maeda K, Eguchi M, Youngblood WJ, Mallouk TE (2008) Chem Mater 20:6770
298. Tong Z, Takagi S, Shimada T, Tachibana H, Inoue H (2006) J Am Chem Soc 128:684
299. Nabetani Y, Takamura H, Hayasaka Y, Shimada T, Takagi S, Tachibana H, Masui D, Tong Z, Inoue H (2011) J Am Chem Soc 133:17130
300. Nakato T, Yamashita Y, Kuroda K (2006) Thin Solid Films 495:24
301. Miyamoto N, Yamamoto S, Shimasaki K, Harada K, Yamauchi Y (2011) Chem Asian J 6:2936
302. Iler RK (1966) J Colloid Interface Sci 21:569
303. Decher G (1997) Science 277:1232
304. Kleinfeld ER, Ferguson GS (1994) Science 265:370
305. Sasaki T, Ebina Y, Watanabe M, Decher G (2000) Chem Commun 2163
306. Wang L, Omomo Y, Sakai N, Fukuda K, Nakai I, Ebina Y, Takada K, Watanabe M, Sasaki T (2003) Chem Mater 15:2873
307. Zhao J, Kong X, Shi W, Shao M, Han J, Wei M, Evans DG, Duan X (2011) J Mater Chem 21:13926
308. Sakai N, Fukuda K, Omomo Y, Ebina Y, Takada K, Sasaki T (2008) J Phys Chem C 112:5197
309. Liu M, Wang T, Ma H, Fu Y, Hu K, Guan C (2014) Sci Rep 4:7147
310. Keller SW, Johnson SA, Brigham ES, Yonemoto EH, Mallouk TE (1995) J Am Chem Soc 117:12879
311. Akatsuka K, Ebina Y, Muramatsu M, Sato T, Hester H, Kumaresan D, Schmehl RH, Sasaki T, Haga MA (2007) Langmuir 23:6730
312. Wang L, Sasaki T, Ebina Y, Kurashima K, Watanabe M (2002) Chem Mater 14:4827
313. Wang L, Ebina Y, Takada K, Sasaki T (2004) Chem Commun (Camb) 1074
314. Li L, Ma R, Iyi N, Ebina Y, Takada K, Sasaki T (2006) Chem Commun (Camb): 3125
315. Blodgett KB (1935) J Am Chem Soc 57:1007
316. Yamaki T, Asai K (2001) Langmuir 17:2564
317. Umemura Y, Yamagishi A, Schoonheydt R, Persoons A (2002) J Am Chem Soc 124:992
318. Muramatsu M, Akatsuka K, Ebina Y, Wang KZ, Sasaki T, Ishida T, Miyake K, Haga M (2005) Langmuir 21:6590
319. Saruwatari K, Sato H, Idei T, Kameda J, Yamagishi A, Takagaki A, Domen K (2005) J Phys Chem B 109:12410
320. Li BW, Osada M, Ozawa TC, Ebina Y, Akatsuka K, Ma RZ, Funakubo H, Sasaki T (2010) ACS Nano 4:6673
321. Shibata T, Fukuda K, Ebina Y, Kogure T, Sasaki T (2008) Adv Mater 20:231
322. Tetsuka H, Takashima H, Ikegami K, Nanjo H, Ebina T, Mizukami F (2009) Chem Mater 21:21
323. Jung C, Ohnishi T, Osada M, Takada K, Sasaki T (2013) ACS Appl Mater Interfaces 5:4592
324. Shibata T, Ohnishi T, Sakaguchi I, Osada M, Takada K, Kogure T, Sasaki T (2009) J Phys Chem C 113:19096
325. Miyamoto N, Nakato T (2002) Adv Mater 14:1267
326. Gabriel J-CP, Davidson P (2003) Top Curr Chem 226:119
327. Nakato T, Miyamoto N (2009) Materials 2:1734
328. Miyamoto N, Nakato T (2012) Isr J Chem 52:881
329. Paineau E, Antonova K, Baravian C, Bihannic I, Davidson P, Dozov I, Impéror-Clerc M, Levitz P, Madsen A, Meneau F, Michot LJ (2009) J Phys Chem B 113:15858
330. Nakato T, Nono Y, Mouri E, Nakata M (2014) Phys Chem Chem Phys 16:955
331. Nakato T, Miyamoto N, Harada A, Ushiki H (2003) Langmuir 19:3157
332. Mochizuki D, Kumagai K, Maitani MM, Wada Y (2012) Angew Chem Int Ed 51:5452
333. Mochizuki D, Kumagai K, Maitani MM, Suzuki E, Wada Y (2014) J Phys Chem C 118:22968

334. Pickering SU (1907) J Chem Soc Trans 91:2001
335. Aveyard R, Binks BP, Clint JH (2003) Adv Colloid Interface Sci 100–102:503
336. Abend S, Bonnke N, Gutschner U, Lagaly G (1998) Colloid Polym Sci 276:730
337. Ashby NP, Binks BP (2000) Phys Chem Chem Phys 2:5640
338. Yang F, Liu S, Xu J, Lan Q, Wei F, Sun D (2006) J Colloid Interface Sci 302:159
339. Nakato T, Ueda H, Hashimoto S, Terao R, Kameyama M, Mouri E (2012) ACS Appl Mater Interfaces 4:4338
340. Imperiali L, Liao KH, Clasen C, Fransaer J, Macosko CW, Vermant J (2012) Langmuir 28:7990
341. Mejia AF, Diaz A, Pullela S, Chang Y-W, Simonetty M, Carpenter C, Batteas JD, Mannan MS, Clearfield A, Cheng Z (2012) Soft Matter 8:10245